NAVAL POSTGRADUATE SCHOOL
Monterey, California

THESIS

AN APPLICATION OF A NUMERICAL SEA ICE MODEL

TO THE EAST GREENLAND AREA

by

Walter B. Tucker III

December 1981

Thesis Advisor: R. L. Haney

Approved for public release; distribution unlimited

REPORT DOCUMENTATION PAGE

READ INSTRUCTIONS BEFORE COMPLETING FORM

1. REPORT NUMBER

2. GOVT ACCESSION NO.

3. RECIPIENT'S CATALOG NUMBER

4. TITLE (and Subtitle)
An Application of a Numerical Sea Ice Model to the East Greenland Area

5. TYPE OF REPORT & PERIOD COVERED
Master's Thesis
December, 1981

6. PERFORMING ORG. REPORT NUMBER

7. AUTHOR(s)
W. B. Tucker III

8. CONTRACT OR GRANT NUMBER(s)

9. PERFORMING ORGANIZATION NAME AND ADDRESS
Naval Postgraduate School
Monterey, California 93940

10. PROGRAM ELEMENT, PROJECT, TASK AREA & WORK UNIT NUMBERS

11. CONTROLLING OFFICE NAME AND ADDRESS
Naval Postgraduate School
Monterey, California 93940

12. REPORT DATE
December, 1981

13. NUMBER OF PAGES
109

14. MONITORING AGENCY NAME & ADDRESS(if different from Controlling Office)

15. SECURITY CLASS. (of this report)
UNCLASSIFIED

15a. DECLASSIFICATION/DOWNGRADING SCHEDULE

16. DISTRIBUTION STATEMENT (of this Report)
Approved for public release: distribution unlimited

17. DISTRIBUTION STATEMENT (of the abstract entered in Block 20, if different from Report)

18. SUPPLEMENTARY NOTES
Funding for this research was provided by the Arctic Program, Office of Naval Research and the U.S. Army Cold Regions Research and Engineering Laboratory.

19. KEY WORDS (Continue on reverse side if necessary and identify by block number)
Sea ice, East Greenland, modeling, ice drift, ice growth

20. ABSTRACT (Continue on reverse side if necessary and identify by block number)
A dynamic-thermodynamic sea ice model which employs a viscous-plastic constitutive law has been applied to the East Greenland area. The model is run on 40-km spatial scale at 1/4-day time steps for a 60-day period with forcing data beginning on 1 October 1979. Results tend to verify that the model predicts reasonable thicknesses and velocities within the ice margin. Thermodynamic ice growth produces excessive ice extent, however, probably due to inadequate parameterization of oceanic heat flux. Ice velocities near the free ice edge are also not well simulated, and preliminary investigations attribute this to

20.
an improper wind field in this area. A simulation which neglects ice strength, effectively damping ice interaction with itself and allowing no resistance to deformation, produces excessive ice drift toward the coast and results in unrealistic nearshore thicknesses. A dynamics-only simulation produced reasonable results including a more realistic ice extent, but the need for proper thermodynamics is also apparent. Other simulations verify that ice import from the Arctic Basin, and ice transport due to winds and currents, were also important components in the model studies.

Approved for public release: distribution unlimited

An Application of a Numerical Sea Ice Model to the East Greenland Area

by

Walter B. Tucker III
U.S. Army Cold Regions Research and Engineering Laboratory
B.S., Virginia Polytechnic Institute, 1968

Submitted in partial fulfillment of the
requirements for the degree of

MASTER OF SCIENCE IN METEOROLOGY

from the

NAVAL POSTGRADUATE SCHOOL

December, 1981

ABSTRACT

A dynamic-thermodynamic sea ice model which employs a viscous-plastic constitutive law has been applied to the East Greenland area. The model is run on a 40-km spatial scale at 1/4-day time steps for a 60-day period with forcing data beginning on 1 October 1979. Results tend to verify that the model predicts reasonable thicknesses and velocities within the ice margin. Thermodynamic ice growth produces excessive ice extent, however, probably due to inadequate parameterization of oceanic heat flux. Ice velocities near the free ice edge are also not well simulated, and preliminary investigations attribute this to an improper wind field in this area. A simulation which neglects ice strength, effectively damping ice interaction with itself and allowing no resistance to deformation, produces excessive ice drift toward the coast and results in unrealistic nearshore thicknesses. A dynamics-only simulation produced reasonable results including a more realistic ice extent, but the need for proper thermodynamics is also apparent. Other simulations verify that ice import from the Arctic Basin, and ice transport due to winds and currents, were also important components in the model studies.

TABLE OF CONTENTS

LIST OF FIGURES

LIST OF TABLES

ACKNOWLEDGMENTS

The author is indebted to Dr. W.D. Hibler III for providing the computer code, ice growth rates and much guidance in the early stages of this work. The guidance, encouragement and comments provided by Professors R.L. Haney and R.G. Paquette are also gratefully acknowledged. The author also thanks Mr. E. Perkins and Mr. M. Pacillo for much time-consuming figure preparation, and especially Ms. D. Harp for an excellent job of typing the manuscript. The funding which made this research possible, provided by the Arctic Program, Office of Naval Research, and the U.S. Army Cold Regions Research and Engineering Laboratory, is greatly appreciated.

I. INTRODUCTION

The Greenland Sea is an area of confluence for polar and temperate systems for both atmosphere and ocean. In the atmosphere, migratory cyclones which were formed over or adjacent to the North American continent track through and frequently undergo cyclolysis in the Greenland and Norwegian Seas. These dying cyclones give rise to the Icelandic Low (Sanders and Gyakum, 1980), a low pressure feature apparent in Northern Hemisphere climatological analyses. In the hydrosphere, the area is characterized by a complex system of currents resulting from the meeting of the warm North Atlantic current, a Gulf Stream outflow which flows into the Arctic Basin west of Spitsbergen, and the cold East Greenland current flowing southward out of the Arctic Basin along the Greenland coast.

Along with colder and less dense water that is transported into the region by the East Greenland current, sea ice is advected out of the Arctic Basin. This ice transport is greatly assisted and possibly dominated by the generally northerly winds which result from the cyclones transiting and stagnating over the Greenland and Norwegian Seas. In addition, the ocean surface heat balance is favorable for the production of new ice here during the winter months, a factor which further increases the ice extent during this period. Likewise, summer warming ablates the ice being transported south, resulting in a greatly reduced ice extent. The presence of this seasonally varying sea ice cover results in a system of highly complex air-sea interactions and feedback effects that are not well understood.

The East Greenland area is also of interest to many nations for economic and military reasons. The presence of sea ice severely hampers surface navigation, affecting both commercial maritime and fishing industries. In addition, subsurface navigation is affected by sea ice because of its influence on the acoustic regime. Hydroacoustic instrumentation is influenced by ice scattering and high ambient noise levels due to ice floe collisions and deformation (Kozo and Diachok, 1973; Diachok and Winokur, 1974).

That there is a need to understand the effect of sea ice on oceanic and atmospheric processes is obvious. A logical first step, however, is to attempt to understand which processes control the presence and variability of the sea ice in this region. With this understanding, atmospheric and oceanic models could be improved by including the response of the ice cover to predicted results, thereby implementing crude feedback mechanisms. Later, coupling of these models would begin to delineate the more complex processes.

It is well known that the major components which govern the sea ice balance in any ice-covered region are the thermodynamic balance at the sea surface, the air and water stresses upon the ice, the Coriolis force and the internal ice stress (the stress transmitted by the ice itself). Consideration of the East Greenland area as a separate entity also requires that the flux of ice into the region from the Arctic Basin be included as a component in the mass balance of ice. The role of each of these components with respect to the East Greenland region has not been made clear.

Previous studies of the ice balance in this region have focused primarily on variations in ice extent. Both seasonal and interannual

variations have been examined in these predominantly climatological studies. Vowinckel (1964) concludes that the interannual variations in ice extent are less than seasonal variations. He reasons that potentially large year-to-year variations are generally counterbalanced by extremes in freezing and thawing (i.e. the greater the extent in April, the greater the reduction of ice by melting in the summer). His study also concluded that, on the average, seasonal variations are due to fluctuations in the amount of ice being imported from the Arctic Basin. He estimated the total southward ice transport for each month by examining ice extent charts and applying simple assumptions concerning freezing and thawing. The transport by wind alone was then estimated by applying Zubov's formula (Zubov, 1945) to monthly pressure differences at certain latitudes. The transport attributable to currents was taken to be the difference of the total and wind transports. These calculations showed that currents dominated the ice transport during the winter (September-April), with the wind-caused transport being approximately half that of the current transport during that period.

Skov (1970) believes that year-to-year variations in ice extent are caused by ocean current variations. In particular, the fluctuations in the flows of Polar and Atlantic water into the Greenland Sea cause the northward oceanic heat transport to vary, thus influencing the ice extent. Aagaard (1972), on the other hand, found that severe ice years were accompanied by anomalous atmospheric pressure fields. Using Sverdrup dynamics he showed that the southward transport of polar water increased during these anomalous years, bringing unusually large amounts of ice southward. With this reasoning he has attributed anomalous ice extents to variations

in the mean wind and current fields by assuming that the ocean will respond within a reasonable time (several months) to the mean wind stress field. His hypothesis is, moreover, based on local forcing.

Other large scale climatic studies have related the ice extent to various atmospheric parameters. Walsh and Johnson (1979) designed a study to assess interactions of the sea ice and the atmosphere by cross correlating meteorological and ice extent fields which were represented by empirical orthogonal functions. In the examination of these first-order feedback effects, they found that the ice extent responded more strongly to atmospheric forcing occurring one to two months previously than did the atmosphere to the ice for any lag or lead time during an ice retreat period (summer). During the ice advance period, however, the best correlations occurred with zero lag (indicating immediate forcing), and atmospheric response to ice extent was equally as strong as the ice extent response to the atmosphere. The meteorological variable showing the highest correlation with ice extent was generally the surface temperature field. In a different study, which examined specific meteorological features, Kelly (1978) suggested that ice extent in the Greenland Sea may be closely related to the position of the Icelandic Low.

That both local winds and ice production play a major role in ice extent was promoted by Einarsson (1972). He points out that since drifting ice stations often moved across the assumed strong current along the Belgica Bank of northeast Greenland, the wind must be significantly influencing the ice drift. In calculating an annual ice mass budget, he found that export out of the Denmark Strait exceeded the inflow at 76°N, thus the region must be a net producer of ice. He also agrees with Vowinckel (1964)

in finding that winter drift rates are much greater than those of other seasons due to a stronger northeasterly pressure gradient.

Short term rapid advances of the ice edge have been attributed to different mechanisms. For instance, Einarsson (1972) cites specific studies which have found a correlation between rapid advances of ice in the vicinity of Iceland and tongues of low salinity water preceding the ice advance. A rapid advance feature which has been noted for centuries by fishermen occurs frequently in the vicinity of Jan Mayen. This feature consists of a large cape-like extension of ice (aptly named Odden) which protrudes northeastward, delineating a bay of open water to the northwest (Nordbukta). Vinje (1977) believes that the causes of this rapid advance are a weakened Icelandic Low (which would lessen the easterly winds) and a well developed oceanic circulation (which would transport the ice to the east). In a separate study Sanderson (1971) found that rapid advances of the ice edge in the Greenland Sea were not accounted for by monthly mean winds, currents or ice growth rates. Instead, he found a significant correlation between ice edge advance and the monthly mean wind anomaly from the northwest quadrant. This anomaly, which constitutes the departure of the wind from its normal value, presumably boosts the southeasterly branch of the East Greenland Current, thus stimulating a large ice transport to the east.

In addition to these synoptic scale processes which contribute to ice drift and extent, Wadhams (1980a) points out that smaller scale processes may contribute significantly to the ice extent. He believes that wave-induced pulverization of ice near the edge in conjunction with an off-ice wind would cause the pulverized ice to melt very rapidly. This process may

cause a large enough effect to warrant parameterization in a model which predicts the ice edge location. He also points out that baroclinic eddies associated with an unstable oceanic Polar Front may cause rapid disintegration of ice. This ablation proceeds by the eddies drawing floes into the warmer ocean where melting is significant and by moving floes into the proximity of wave action where pulverization and subsequent melting take place.

All of the above investigations have found results which indicate that all major components in the ice balance are important. The question of relative importance of the terms remains, however. Because there are limits to what can be resolved by empirical studies in this region (due primarily to sparseness and low accuracy of observational data), it seemed that an ice modeling study might be useful. The idea of this type of investigation would be to attempt to sort out the major processes through a series of model sensitivity tests.

Karlsson (1969) formulated the physical framework for a sea ice model applicable to the East Greenland Sea. This theoretical framework considered all terms in the momentum balance and treated the ice as an isotropic elastic medium to obtain the internal ice stresses. In addition, a continuity equation accounted for ice concentration and allowed for growth and ablation. Unfortunately, this model was never taken beyond the formulation stage. In addition to Karlsson's modeling efforts several Russian investigators have applied simple ice balance models to the East Greenland region (Lebedev and Uralov, 1976; Antropova and Kogan, 1977). These models basically estimated the major components affecting the ice balance (inflow,

outflow and growth) but without a proper treatment of the actual ice dynamics within the region.

This thesis presents the results of an application of a dynamic-thermodynamic sea ice model to the East Greenland area. Preliminary results of this work have previously been reported by Tucker and Hibler (1981). Further analyses and the results of various sensitivity tests are reported here. This effort represents the first attempt to apply a complete sea ice model specifically to the East Greenland area.

II. MODEL DESCRIPTION AND APPLICATION

The sea ice model utilized in this study is a two-thickness-level, viscous-plastic model which was developed by Hibler (1979). This particular model was selected for use in this study because it has previously yielded very reasonable results in Arctic Basin studies (Hibler, 1979) and because the numerical code has been documented (Hibler, 1980a) and can be applied to any specific region with relative ease.

Basic components of the model include a momentum balance, a constitutive law, an ice thickness distribution, an ice strength parameterization and a thermodynamic balance.

The momentum equation for ice floating on an ocean is

$$m \frac{d\underset{\sim}{u}}{dt} = \underset{\sim}{C} + \underset{\sim}{\tau}_w + \underset{\sim}{\tau}_a + \underset{\sim}{F} + \underset{\sim}{G} + \underset{\sim}{T} \tag{1}$$

where $\underset{\sim}{u}$ is the ice velocity, m is the ice mass per unit area, $\underset{\sim}{C}$ is the Coriolis force, $\underset{\sim}{\tau}_w$ and $\underset{\sim}{\tau}_a$ are the water and air stresses, $\underset{\sim}{F}$ is the force due to internal ice stress variations, $\underset{\sim}{G}$ is force due to long term geostrophic currents and $\underset{\sim}{T}$ is the force attributed to the tilt of the ocean surface. The acceleration term ($m\, d\underset{\sim}{u}/dt$), a total derivative, is further broken into the local acceleration plus momentum advection.

The constitutive law is of the form

$$\sigma_{ij} = f(\dot{\varepsilon}_{ij}, P, \zeta, \eta) \tag{2}$$

where σ_{ij} is a two-dimensional stress tensor, $\dot{\varepsilon}_{ij}$ is the strain rate tensor and P is a pressure term representing ice strength, which depends

upon the ice thickness distribution. ζ and η are nonlinear shear and bulk viscosities and their values depend on $\dot{\varepsilon}_{ij}$ and P in accordance with a viscous-plastic rheology. The details of this constitutive law are presented by Hibler (1979). The law in this form allows the ice to deform as a linear viscous (Newtonian) fluid at small strain rates but yields as a purely plastic material at higher strain rates. The usual or normal range of strain rates causes frequent plastic yielding as manifested by pressure ridge and lead formation. Once the stress tensor is obtained from the constitutive relationship, the force components due to internal ice stress are calculated from

$$F_i = \partial \sigma_{ij} / \partial x_j \tag{3}$$

The ice strength parameterization couples the ice strength to the thickness distribution. The ice strength pressure term P in equation (2) is a function of thickness and compactness (concentration) according to

$$P = P^* \, h \exp [-C(1-A)] \, . \tag{4}$$

Here P* and C are fixed empirical constants, h is the average ice thickness for the grid cell and A is the compactness which represents the fractional area of the grid cell (varying from 0.0 to 1.0) covered by ice of thickness h.

The evolution of ice thickness and compactness is governed by two continuity equations:

$$\frac{\partial h}{\partial t} = - \frac{\partial (uh)}{\partial x} - \frac{\partial (vh)}{\partial y} + S_h + \text{diffusion} \tag{5}$$

$$\frac{\partial A}{\partial t} = - \frac{\partial (uA)}{\partial x} - \frac{\partial (vA)}{\partial y} + S_A + \text{diffusion} \tag{6}$$

where u and v are velocity components in the x and y directions and S_h and S_A are thermodynamic terms which govern the ice thickness and concentration due to growth and decay. The diffusion terms are necessary for numerical stability. The thickness and compactness of ice in each grid cell are determined by equations (5) and (6) for each time step. The remainder of the grid cell (fractionally, 1-A) is considered to be open water.

A surface heat balance equation, together with a simple thermodynamic ice model, were used to calculate the growth rates, S_h, in the manner described by Hibler (1980b). The balance equation included terms for incoming long and short wave radiation, outgoing long wave radiation, sensible and latent heat fluxes and ice conductivity. The external data required to solve this equation came from the National Climatological Center's (NCC) daily analyzed fields (temperature, humidity and pressure) and from climatological estimates (cloudiness). Radiation values were calculated as described by Hibler (1980b). In a separate run, the ice growth rates were calculated for each grid point at 0.5-m thickness levels (Hibler, pers. comm.), then stored for later access by the model which interpolated a growth rate to the proper thickness level. The change in compactness due to growth and decay, S_A, is calculated as detailed by Hibler (1979). This effect is parameterized so as to allow the amount of open water (or very thin ice) to rapidly decrease under growth conditions and to slowly increase during periods of melting.

Initial simulation runs which tested only the thermodynamic portion of the numerical code found ice growth to be excessive. This was presumably due to the lack of oceanic heat flux. Water temperature in the heat

balance equation was specified to be 271.2 K, the freezing point of seawater. This implies that no ice ablation as a result of either boundary layer heat storage or advection of warmer waters into this area occurs. In light of this, a crude oceanic heat flux was incorporated by adding a 0.1-m-per-day decay rate to the thin ice growth rates east of a fixed boundary in the grid area. West of this boundary this melt rate supplement falls off in a cosine manner until, finally, no modification is made to the growth rates. The idea of establishing this zone was to attempt to crudely simulate the oceanic Polar Front, which roughly follows the ice margin, having relatively warm waters to the east and below-freezing temperatures to the west (Wadhams et al., 1979; Aagaard and Coachman, 1968). The position of this zone within the model grid is shown in Figure 1. It was positioned roughly according to the location of the ice edge at the end of November 1979.

The air and water stresses as shown in the momentum equation (1) were calculated from simple nonlinear drag laws which assumed constant turning angles and required geostrophic winds and ocean currents. Winds were calculated from NCC daily analyzed sea level pressure fields. Currents, as well as ocean tilt, were determined from a temporally constant dynamic height field (Syd Levitus, pers. comm.). These fields are discussed further in the Results and Discussion section.

The overall flow of the model is shown in Figure 2. The simultaneous equations (1), (4), (5) and (6) are solved by finite difference techniques using a staggered grid procedure. The momentum equation (1) is solved by a semi-implicit predictor-corrector technique with velocities being calculated by over-relaxation for each of the two time steps. The thickness and

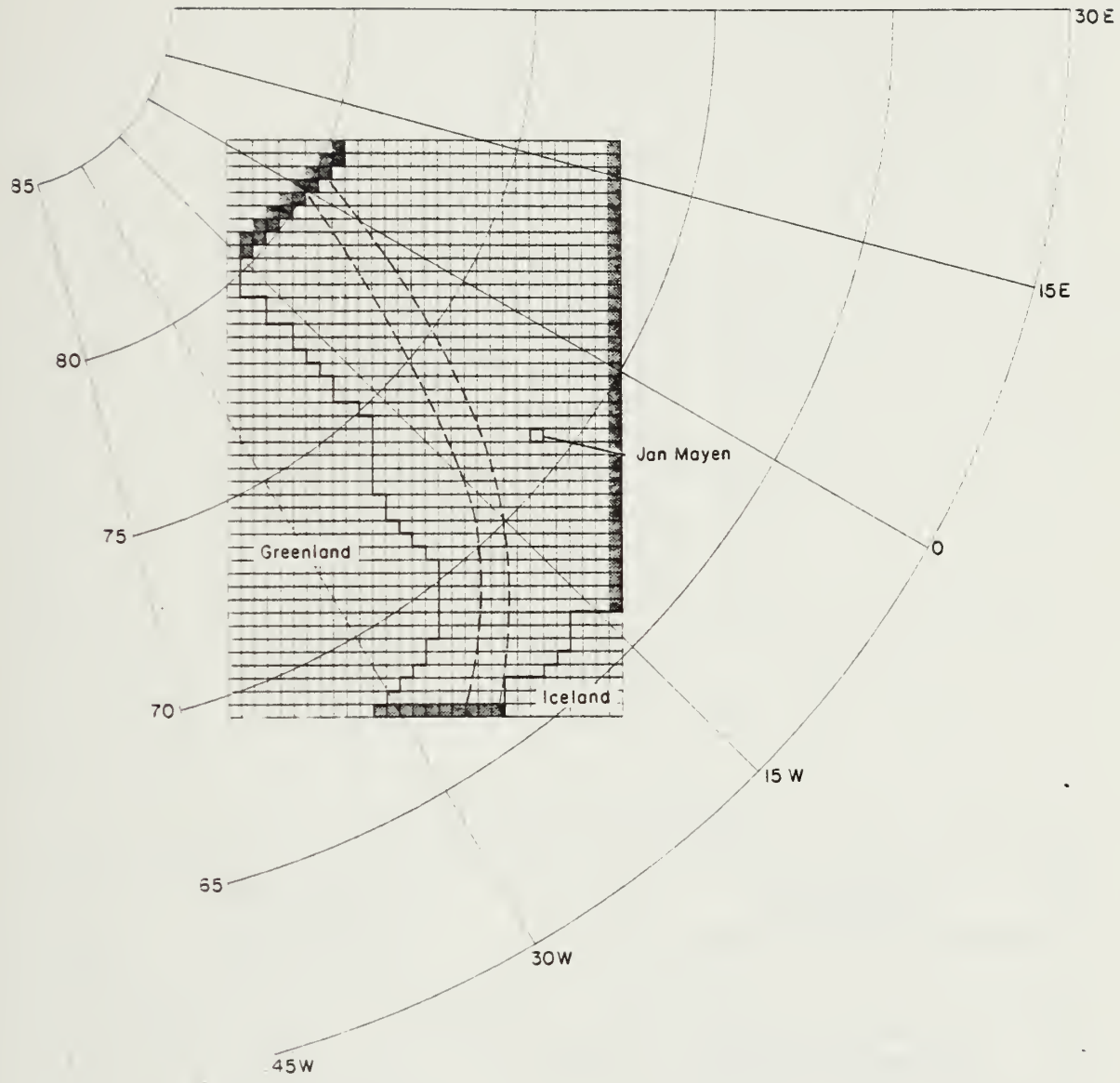

Figure 1. Model grid with solid and free boundaries (shaded). Dashed lines represent boundaries of the oceanic heat flux parameterization.

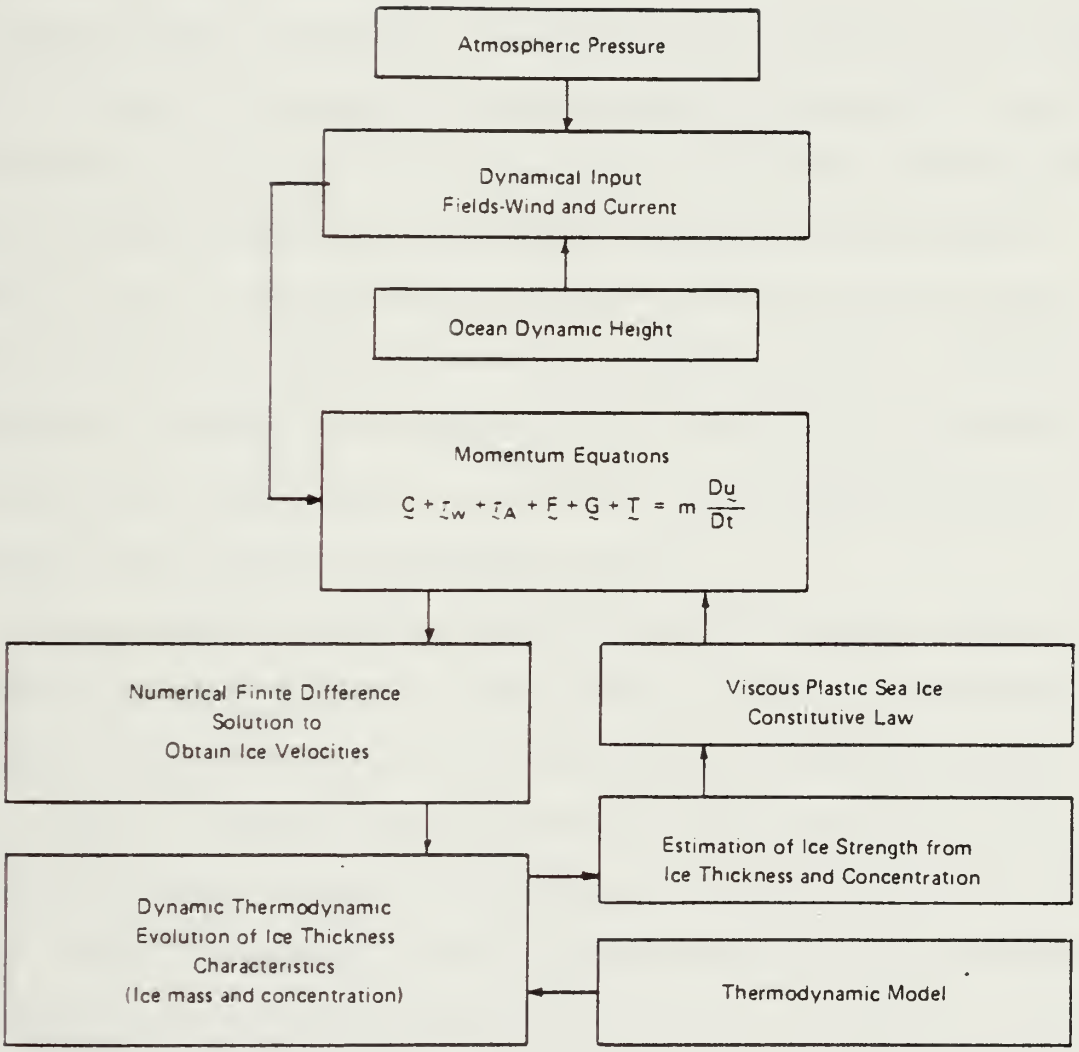

Figure 2. Model flow (after Hibler, 1980a).

compactness continuity equations are solved explicitly with a modified Euler step.

A 40-km, 31x45 grid covering the East Greenland area was established for the simulations. A Lambert azimuthal equivalent projection provided grid cells of equal areas. The location of the grid with boundaries is shown in Figure 1. Using the staggered grid procedure, velocities are calculated for the grid points, with thicknesses and compactnesses specified for the cells between the grid points.

The Fram Strait (northwest), the Denmark Strait (south) and the entire eastern boundary are designated as open boundaries (through which inflow and outflow can take place). For ice strength calculations, the ice thickness of the open boundary cells in the Denmark Strait and the eastern boundary is taken to be the average thickness of adjacent cells located inside the boundary. For the Fram Strait, an inflow region, a different procedure was followed in this investigation. Because this area constitutes the major outflow region for the Arctic Basin, the thicknesses of these cells were specified independent of time.

Velocity values at the solid boundaries are set to zero. With the viscous-plastic rheology, which contains terms to account for compressive and shear stress, effects of the coastline should be adequately reproduced. That is, along-shore shear and high strength areas due to ice thickness build-ups presumably are inherent in the plastic rheology without further boundary stipulations. This was shown to be the case in an Arctic Basin study with this model (Hibler, 1979).

The relatively small grid size (40 km) and large ice velocities in this region required the model to be run at a 1/4-day (21,600-s) time step

to satisfy the Courant-Fredrichs-Levy stability criterion (in this case $\Delta t \leq \Delta x \left[2(u^2 + v^2)\right]^{-1/2}$). Winds and growth rates were interpolated from their daily values to this interval. All other model parameters were identical to those used by Hibler (1979) for the Arctic Basin study with the exception of the Coriolis parameter and P*. For this study, the Coriolis parameter was calculated for each grid point location and, therefore, it varies with latitude. The constant P*, used for the determination of ice strength (eq. 4), was set to four times the value used in the Arctic Basin simulations ($5.0 \cdot 10^3$ N m^{-1}). This change was implemented when initial tests showed ice velocities to be excessive, presumably due to the large magnitudes and variability of the daily wind fields. The previous simulations had used 8-day averaged winds, which inherently provided spatially and temporally smoothed fields.

Because the computer at this facility (U.S. Army Cold Regions Research and Engineering Laboratory) was quite small, the simulations were restricted to a 60-day study period in order to obtain a reasonable turnaround time. This fact limited the scope of this investigation to short term or seasonal effects. The continuous period of October through November, 1979, was chosen for study primarily because it was a period of rapid ice expansion and thus would allow an assessment of the relative importance of dynamics and thermodynamics to the ice expansion. In addition, position data for drifting buoys located on the ice were available for this time period (Kloster and Rafto, 1980). Initial ice compactness was digitized from the 2 October 1979 ice chart as published by the Naval Polar Oceanography Center (NPOC, 1979). Thickness for the initial field was estimated by allowing it to vary linearly with latitude, 1.0 m at 67°N to 3.2 m at

83°N. These estimates seemed reasonable based on data reported from submarine transects of the area during different time periods (Kozo and Tucker, 1974; Wadhams, 1980b). Similarly, thickness for the Fram Strait inflow cells, which remained constant for the simulations, was specified to be 3.2 m for the cells nearest the coast and decreased linearly to 0.0 m for the most northeasterly cell.

Various simulations were carried out to assess the response of the model to different forcing processes during this 60-day period. The primary simulation, referred to as the standard simulation (or run), incorporates the entire dynamic-thermodynamic model with forcing fields as described. Other simulations test the sensitivity of the model 1) to thermodynamics alone, 2) to zero ice strength, 3) to zero ice import from the Arctic Basin, 4) to zero currents, 5) to a modified current field, 6) to zero winds and, finally, 7) to ice dynamics alone. The results of these simulations are discussed in the following section.

III. RESULTS AND DISCUSSION

In this section a brief discussion of the current and wind fields will be followed by the various simulation results. Standard simulation results will be discussed at length, followed by brief discussions of each of the sensitivity tests which compare results to the standard run and to observations where possible. In the Summary and Concluding Remarks section, some of the vital results of each simulation are presented in tabular form and the results of all tests are summarized.

A. WIND AND CURRENT FIELDS

The 60-day averaged wind field and the geostrophic current field for the October-November 1979 period of study are shown in Figure 3. The most significant feature of the wind field is the narrow band of generally northerly winds that follows the Greenland coast. The surprising elements are the large topographical influence that Greenland apparently has on the surface pressure field, and the fact that this feature is clearly resolved by the NCC analyzed data which were interpolated from a 2-1/2 degree latitude and longitude grid. As a means of crude verification, the pressure fields were manually compared to those produced independently by Thorndike and Colony (1980) for the same period. In the latter analysis, gridded sea level pressure fields were constructed using an optimal interpolation technique applied to data from approximately 15 drifting buoys in the Arctic Basin and 70 high latitude land stations. The manual comparison showed no major differences between the analyses, and the large pressure gradient along the Greenland coast was also apparent in the Thorndike and

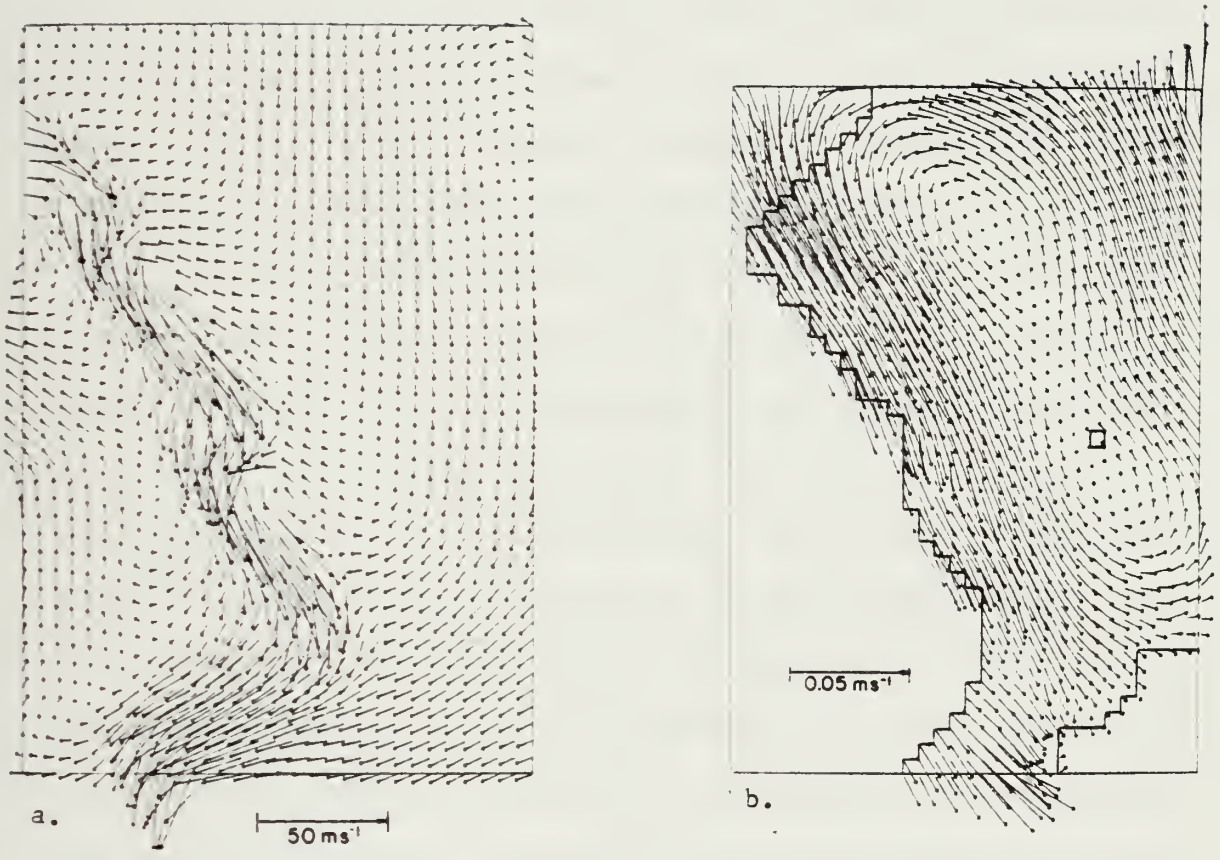

Figure 3. a. 60-day averaged geostrophic wind field.
b. Geostrophic ocean currents.

Colony (1980) analysis. The data from the land stations were used in both analyses, however.

The geostrophic ocean current field appears quite smooth, as would be expected from the fact that a temporally constant dynamic height field was used to calculate these currents. For a crude comparison, late summer currents as compiled by Einarsson (1972) are shown in Figure 4. The geostrophic currents have the same general direction as those of Einarsson, but the magnitudes and specific features differ considerably. For instance, the narrow jet of high velocity currents between Spitsbergen and Greenland are shown to have much higher velocities in the Einarsson compilation. This may be due to the fact that some of Einarsson's data represent instantaneous current measurements whereas the dynamic heights presumably are derived from a long term data base. The question remains, however, as to whether geostrophic currents are representative of actual currents, particularly in the shallower waters adjacent to the Greenland coast. That the flow here may be partially barotropic rather than baroclinic is not out of the question (R. Paquette, pers. comm.). In addition, it is well known that the motion of the ice itself transmits stress into the ocean, modifying the currents over a long time period. These problems concerning actual currents can only be resolved by an extensive observation network or a coupled ice-ocean model. For these reasons, the geostrophic currents which seemingly are a reasonable first order approximation of the currents in this area are used in this study. Simulations described later assess the response of the model to zero currents and to a current field derived from a 60-day average of the ice velocity field.

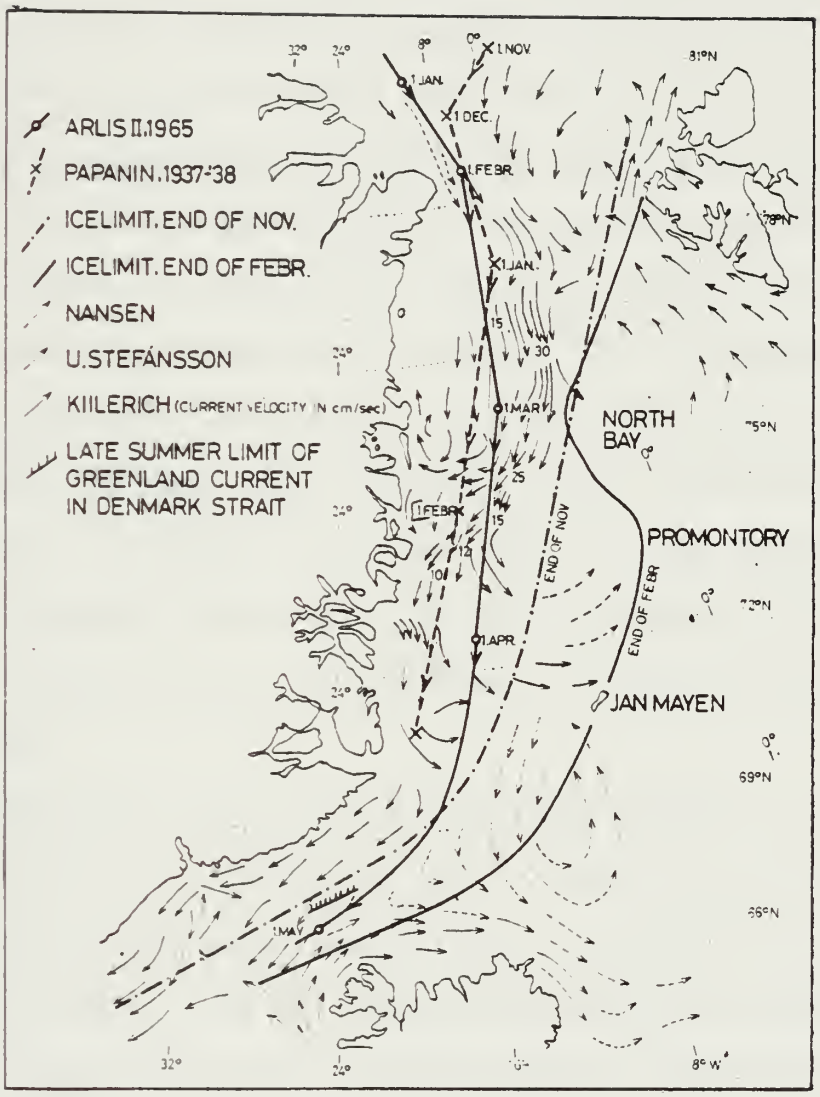

Figure 4. Late summer currents, average ice margins and manned ice station tracks (after Einarsson, 1972).

B. STANDARD SIMULATION

The standard simulation represents the application of the full model over the 60-day time period, with all input parameters as previously described. The idea here was to compare the model results to observations, where possible, to assess the overall validity of the results. In addition, these "benchmark" results are used for comparison to other simulations in which the forcing fields are varied.

Initial and average simulated thickness and compactness fields at 10-day intervals are shown in Figures 5 and 6. The ice edge positions as obtained from the NPOC ice charts for times closely corresponding to the prediction intervals are included in the figures. The 0.2 compactness contour (20% concentration) was chosen to represent the ice edge in the simulated results. Any lower value was found to have a high day-to-day position variability, presumably due to the large variation of the ice growth rates. In addition, this value appeared to correspond well with the 0.1-m average thickness contour, and both seemed to be relatively stable on a day-to-day basis.

These figures clearly show that the predicted ice extent is excessive, particularly after day 10. Although the edge as indicated on the NPOC charts usually enclosed 6-8 oktas (concentration in eighths), the predictions are still excessive, even if a higher concentration is considered as the predicted ice edge to allow for possible resolution errors when the NPOC charts were compiled. Some improvement is noted on day 60 if the predicted edge is taken to be the 0.8 or 1.0 compactness contour, however. It is especially evident on this day because the predicted compactness is much more diffuse than on previous 10-day increments.

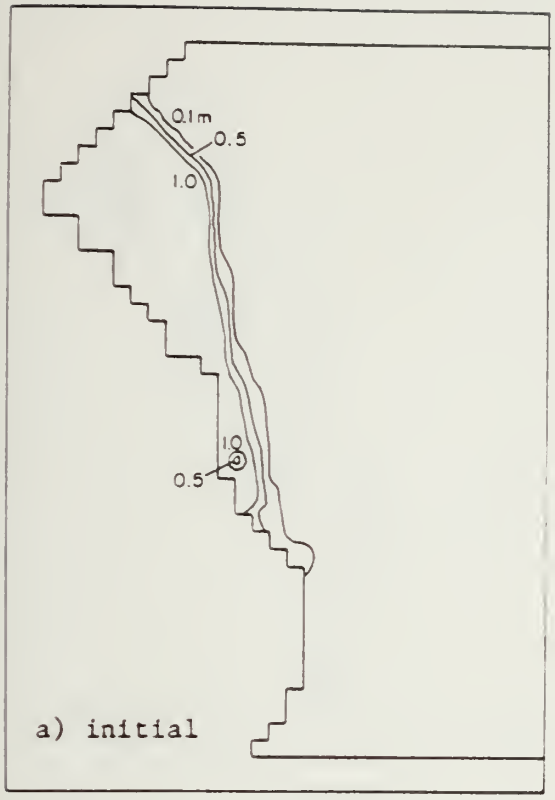

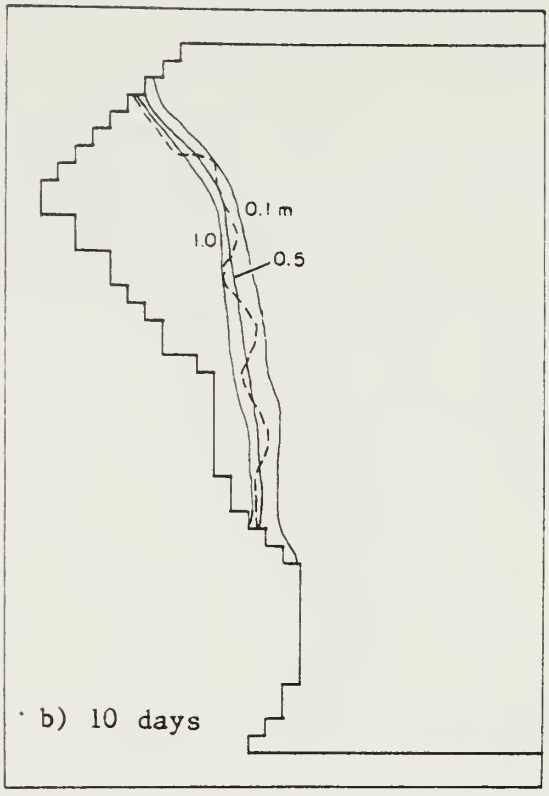

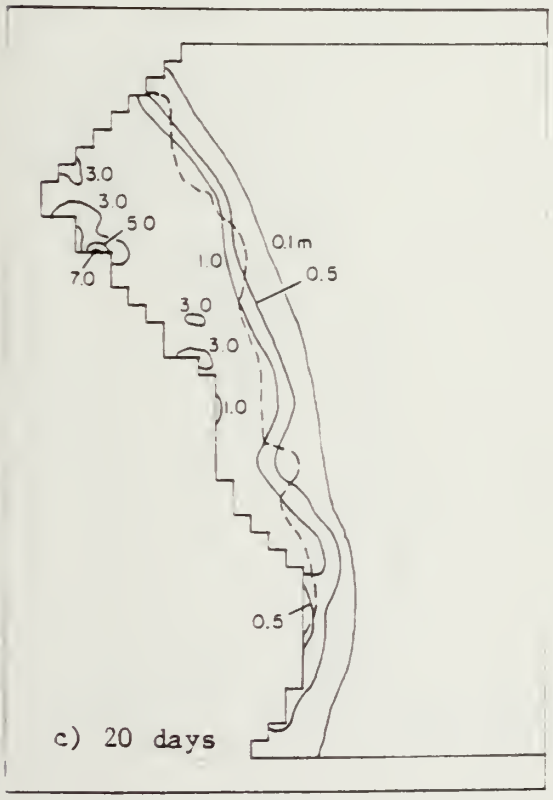

Figure 5. Simulated ice thickness fields. Dashed line is observed ice edge position from NPOC (1979).
a) initial, b) 10 days, c) 20 days.

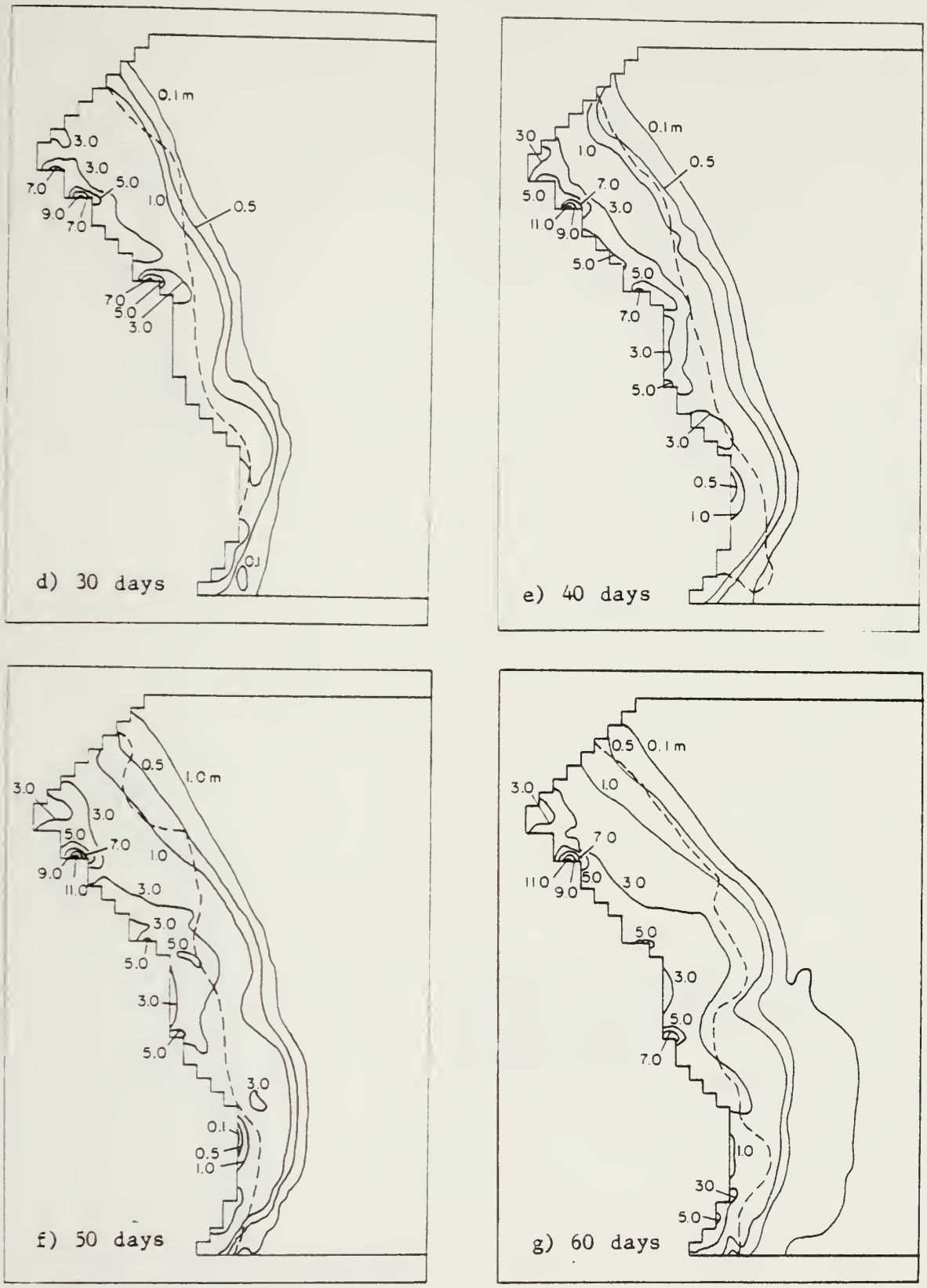

Figure 5 (Con't). d) 30 days, e) 40 days, f) 50 days, g) 60 days.

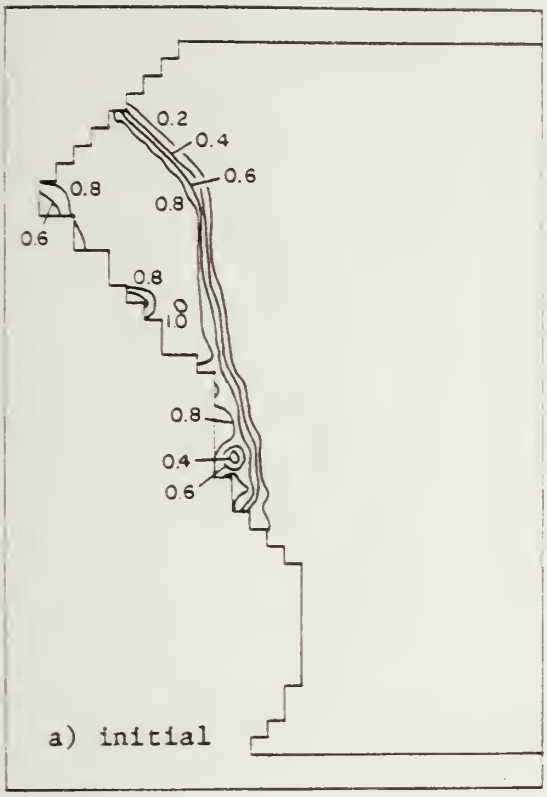

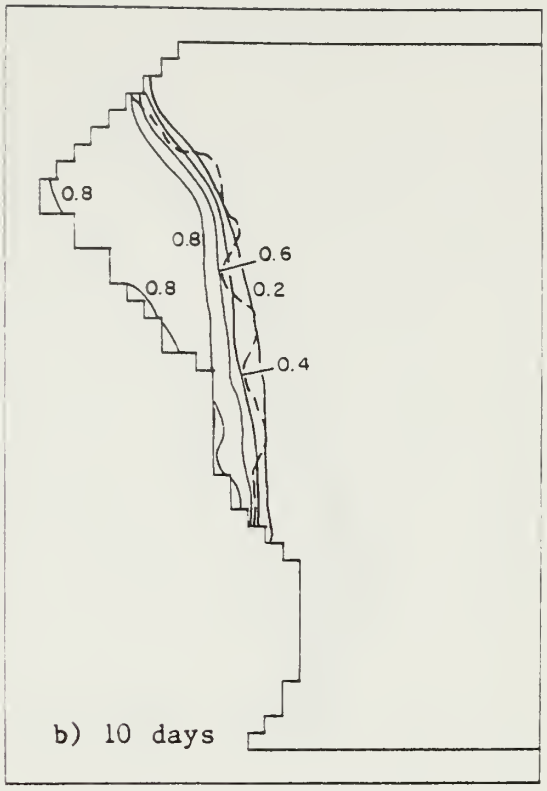

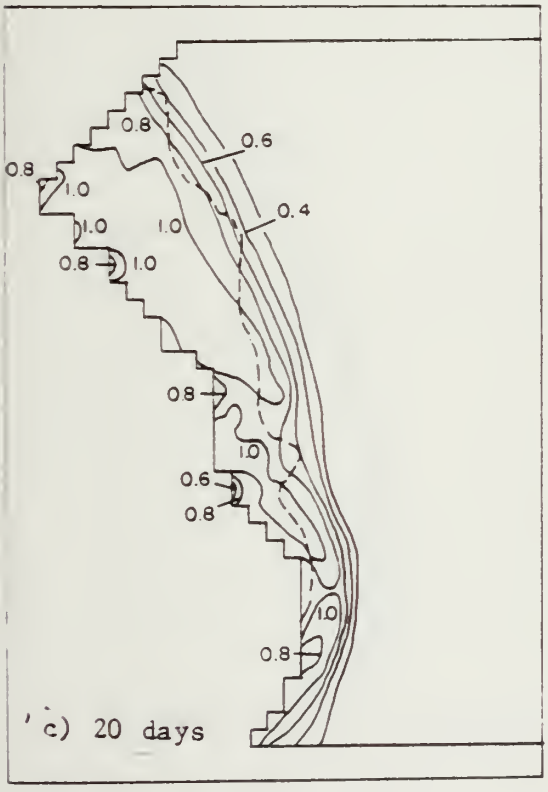

Figure 6. Simulated ice compactness fields. Dashed line is observed ice edge position from NPOC (1979).
a) initial, b) 10 days, c) 20 days.

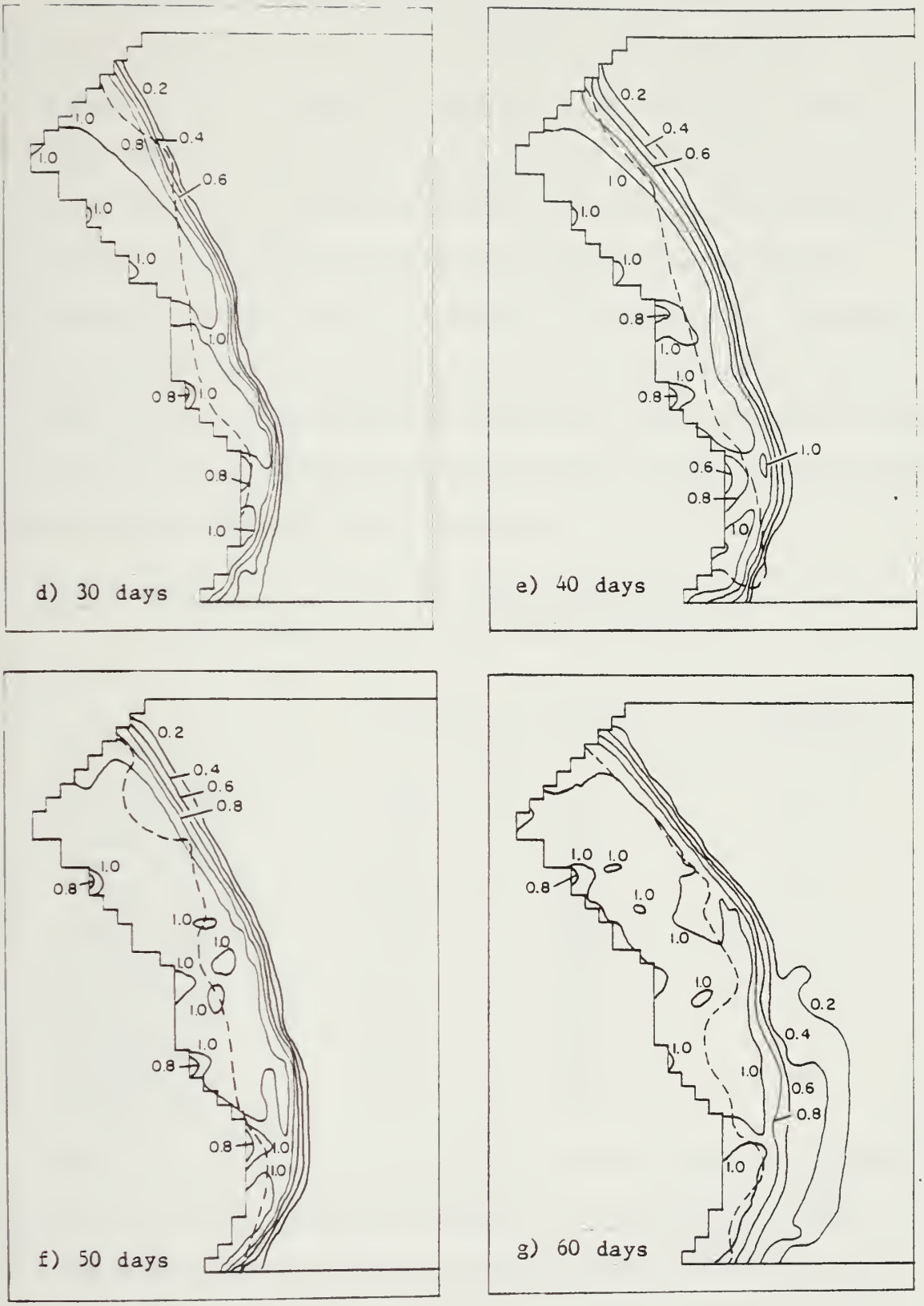

Figure 6 (Con't.) d) 30 days, e) 40 days, f) 50 days, g) 60 days.

A more quantitative comparison of predicted and actual ice extent is presented in Table I. In this table the total ice-covered area as predicted by the model is compared to that estimated from the ice charts for the 10-day intervals. The observed ice coverage was determined by calculating the product of the area covered and the concentration specified on the respective ice chart. The scale of the charts plus the lack of detailed compactnesses limits the accuracy of the calculations; however, the overall comparison in this manner is felt to be meaningful. Table I also shows the percentage difference in predicted versus observed coverage ([predicted-observed]/observed) and the percentage change for both predicted and observed during the 10-day intervals.

Table I. Predicted vs. observed areas (in 10^{11} m^2) of ice cover for 10 day intervals for the standard simulation.

	Predicted	Observed	Difference (%)
Initial Area	1.80	1.80	
Area Day 10	1.88	2.21	-14.9
Change (%)	4.5	22.7	
Area Day 20	3.55	2.24	58.4
Change (%)	88.8	1.4	
Area Day 30	3.38	2.06	64.1
Change (%)	-4.8	-8.0	
Area Day 40	3.79	2.33	62.7
Change (%)	12.1	13.1	
Area Day 50	4.49	2.48	81.0
Change (%)	18.5	6.4	
Area Day 60	5.84	3.13	80.8
Change (%)	30.1	26.2	

Table I verifies that the predicted ice-covered areas are excessive after day 10, and the simulation ends with an ice-covered area excess of 81%. The predicted major expansion occurring between days 10 and 20 is primarily due to large growth rates in the south and east, and this will be

examined further in subsequent simulations. It is interesting to note, however, that after this period, the predicted percentage change in ice-covered area tends to agree with that of the observed. Even the decrease in ice extent between days 20 and 30 is well accounted for by the model.

It appears that the high growth rates are primarily responsible for the large ice extent that is predicted. This reasoning is prompted by the fact that the predicted ice edge after day 10 (Figures 5 and 6) is approximately in the same location as the boundary of the melt rate parameterization discussed previously. Once the ice expands to this limit, then further changes in extent appear to be due to a combination of dynamics and thermodynamics, but the magnitude of the changes is limited by the ocean heat flux parameterization, at least until near the end of the simulation when the growth rates are high enough to overcome the melt rate specification. The upshot is that the growth rates undoubtedly need to include a better parameterization of the oceanic heat flux.

Average ice velocities are also useful in accounting for thickness and compactness variations. Ten-day averaged velocities corresponding to the 10-day intervals of thickness and compactness are shown in Figure 7. Also, the 60-day averaged velocity field is included in this figure (Fig. 7g). While the average velocities for the first 10 days are nearly negligible, those for the remainder of the 10-day intervals closely resemble the average wind field in direction. It is clear that ice dynamics plays some role in the large ice expansion between days 11 and 20, with ice being advected southward by the high velocity stream (near 0.5 m s^{-1}) shown in Figure 7b. As the prescribed geostrophic currents are temporally constant and no larger than 0.05 m s^{-1} (Fig. 3b), this large velocity increase over the

first 10 days can be attributed to winds. Although temperature fields have not been examined in detail, it is likely that these winds also advected lower air temperatures into the southern region of the grid, stimulating a rapid ice expansion. Ice dynamics may also have been partially responsible for the decrease in ice extent between days 21 and 30. The average velocities for this period (Fig. 7c) show a marked onshore component in the vicinity of the ice edge. This velocity configuration would be expected to confine the areal coverage by advecting ice toward the coast. In addition, higher air temperatures from the southeast could be expected to accompany the driving wind field. In contrast, the average velocities for days 41 to 50 and 51 to 60 (Figs. 7e, 7f) show offshore velocity components in this region, which partially accounts for the relatively high ice expansion predicted by the model during these periods. Thus, time variations in the wind forcing appear to produce time variations in ice extent both through direct forcing by ice advection and more indirectly through variable advections of air temperatures.

The ice velocities are also responsible for the predicted thickness and compactness variations occurring near shore that begin to become obvious on day 20 (Figs. 5c, 6c). The coastal thickness build-ups and areas of lesser concentration are obviously the result of ice dynamics because growth rates are very small for ice thicker than 1.0 m and would be expected to have little effect in a 10-day period. The 7.0-m build-up in the northern section of the grid on day 20 (Fig. 5c) continues to increase to 11.0 m by day 40 (Fig. 5e). This appears to be a result of ice impinging upon the promontory here created by the solid boundary. A more detailed look at the ice velocities in this region is presented by Figure

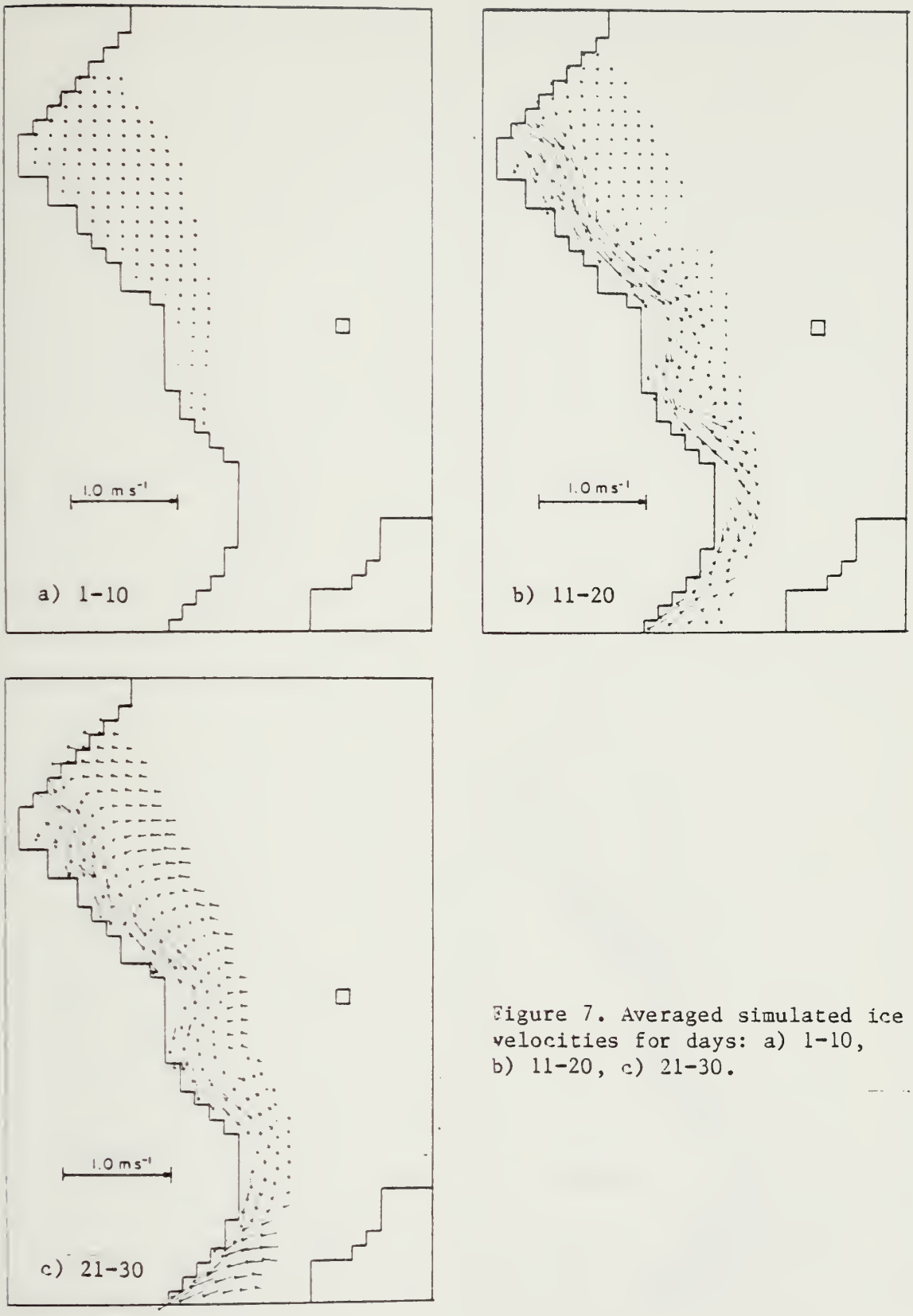

Figure 7. Averaged simulated ice velocities for days: a) 1-10, b) 11-20, c) 21-30.

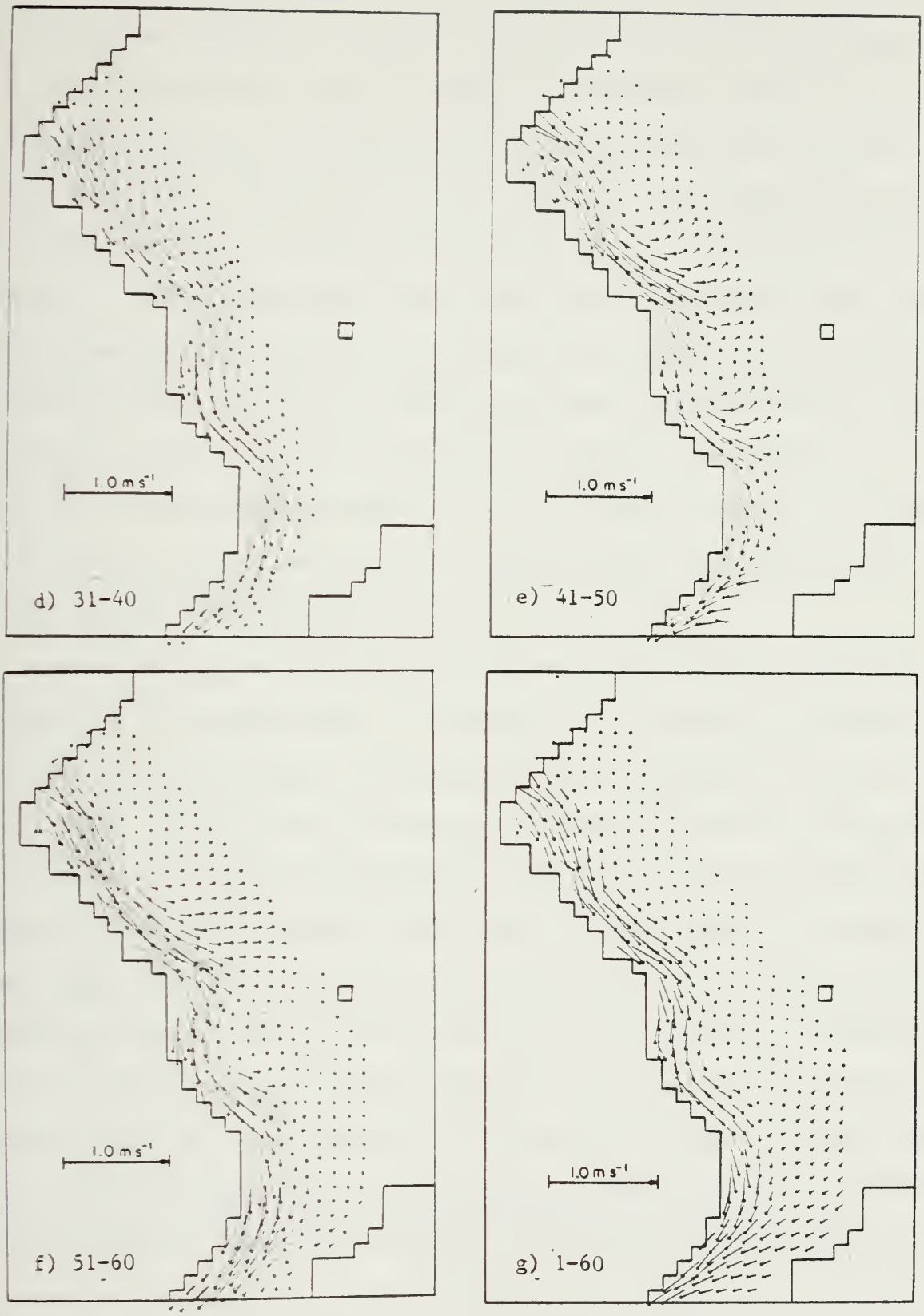

Figure 7 (Con't). d) 31-40, e) 41-50, f) 51-60, g) 1-60.

8, which shows a cross section of 5-day averaged ice velocities for the row of grid points immediately above this large build-up and passing through the entire final width of the ice stream in this region. The thickness build-up, resulting from ice ridging, occurs just beneath the first and second grid points from the left in this figure. The southeastward setting velocities cause the ice to accumulate on the boundary promontory in this region. A similar figure helps explain the lesser concentration area which occurs immediately to the south of the build-up (Fig. 6 c-g). The 5-day velocity averages for a row of grid points beneath the promontory are shown in Figure 9. Once again the velocities are directed southeastward. In this case, however, because there is only a vertical boundary at the coastline, ice is advected away from the coast, eventually resulting in lower concentrations of thinner ice (3.0 m).

These two figures (8 and 9) also demonstrate the effects of the ice strength on the velocity field. In Figure 8, the coastal build-ups have increased the ice strength. This prevents high velocities near shore and also causes the ice to move with more of an offshore component into areas of less strength (smaller thicknesses) as time goes on. At the third grid point, strengths are much less due to lower thickness, and the ice moves at much higher velocities in a more southerly direction. This creates an effective velocity shear in the vicinity of the ice build-up. Further offshore the velocity shear is more likely due to the decreasing winds as distance from the coast increases. In contrast, the coastal velocity shear and offshore turning are barely discernible in Figure 9. These are attributed to the fact that lower strengths are maintained adjacent to the coast

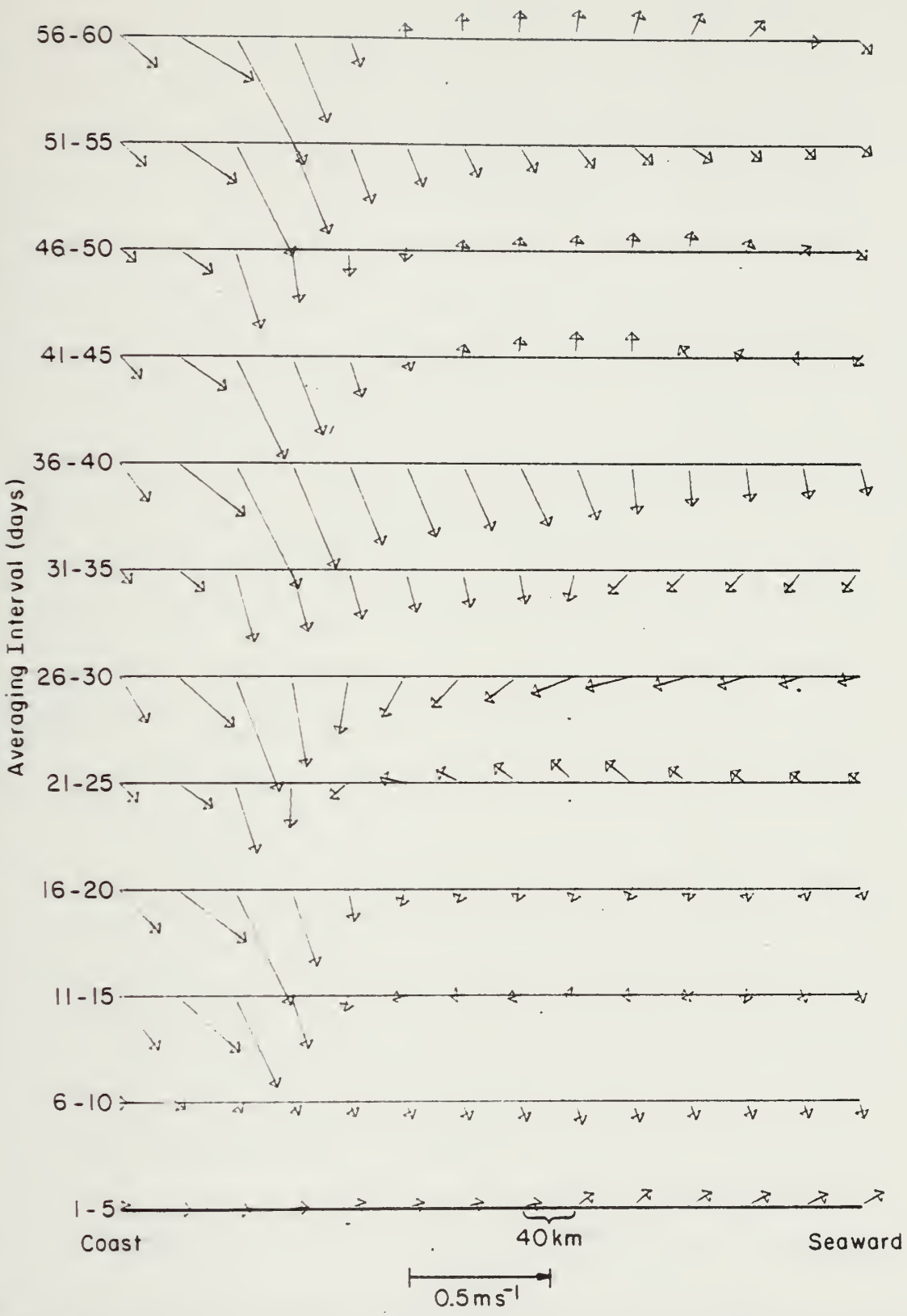

Figure 8. Five-day averaged velocities for the row of grid points immediately above the 11.0-m coastal ice build-up shown in Figure 5g.

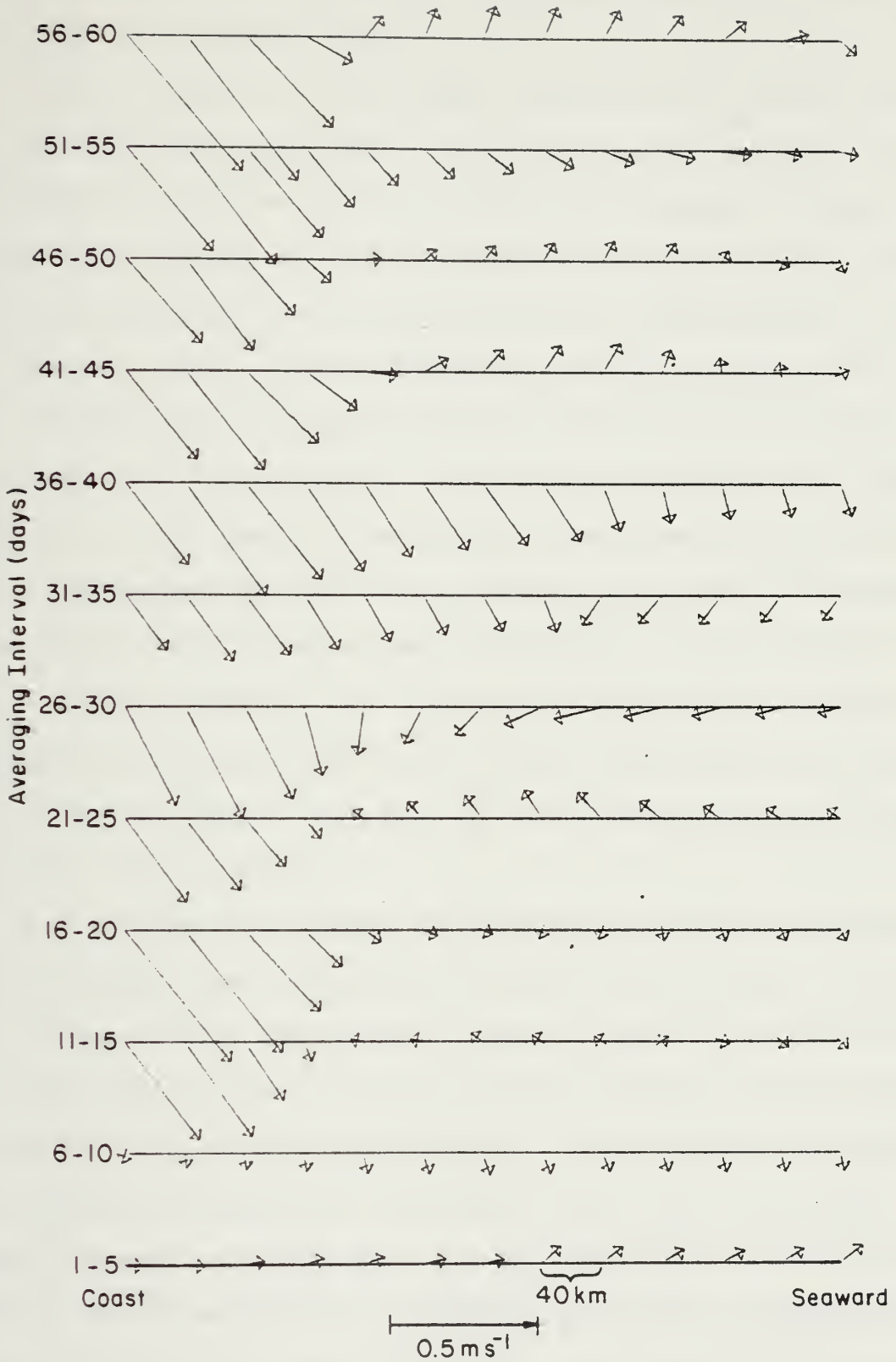

Figure 9. Five-day averaged velocities for the row of grid points immediately below the 11.0-m coastal build-up shown in Figure 5g.

because of relatively low thicknesses and compactnesses. As a result, velocities are not severely affected.

With the exception of the excessive ice extent, the predicted thickness and compactness fields appear to be reasonable and consistent with the specified input fields and with the boundary configuration. Whether major ridging events actually occur in the predicted thickness build-up locations is unknown because there are no data available for these regions. In addition, there is little thickness information available for this entire area. Thicknesses in the northern section of the grid generally agree with those reported by Wadhams (1980b), but it must be remembered that these thicknesses are the result of the specified initial and boundary conditions. Thicknesses and compactnesses increase as the coast is approached in the Denmark Strait region at the end of November in the simulation results (Figs. 5g and 6g). This is consistent with results obtained from an analysis of submarine sonar data collected in March 1971 in this same region (Kozo and Diachok, 1973; Kozo and Tucker, 1974) although absolute thicknesses were not reported.

It is instructive to examine the individual roles that ice import, growth and export have on the total ice volume in this standard simulation. Figure 10 shows the day-to-day change in total ice volume along with the volume of ice produced each day by growth, northern inflow and that exported out of the southern free boundary. Outflow through the eastern free boundary was negligible. This figure clearly shows that thermodynamics (growth) and ice dynamics (northern inflow) are both major contributors to the ice mass balance as simulated by the model. Southern outflow, as expected, only contributes to the balance during the latter part

of the simulation period. Ice growth, northern inflow and southern outflow correlate with the daily volume change with respective coefficients of 0.83, 0.85 and 0.30. These coefficients and Figure 10 imply that growth and inflow had nearly equal roles in the ice mass budget according to the simulation. It is also interesting to note that a 0.48 correlation coefficient exists between the simulated values of daily growth and northern inflow. Two possible explanations may account for this correlation. First, during periods of high northern inflow, winds would be northerly, advecting colder air and stimulating ice growth in lower concentration areas. Second, high northern inflow is likely to be associated with high velocities over the entire grid. This would likely create areas of lesser concentration in which new ice would be rapidly produced. The large variability in northern inflow, including the reversals in flow direction, indicate that the simulated ice transport is primarily wind-induced.

A note of caution concerning inflow is worthwhile at this point. Inflow is partially specified as a boundary condition by the fact that constant thicknesses have been set for the free boundary cells in the Fram Strait. By way of comparison, Aagaard and Greisman (1975) estimated that the ice outflow rate of the Arctic Basin was approximately 0.1 Sv ($3.154 \cdot 10^{12}$ $m^3 yr^{-1}$). The total inflow predicted by the model is $4.73 \cdot 10^{11}$ m^3 for the two-month simulation period. If this value were to remain constant for the entire year, $2.86 \cdot 10^{12}$ m^3 of ice would be imported through the Fram Strait, a value that is 9.1% less than Aagaard's estimate. The simulated inflow may be too high, however. Einarsson (1972), in an investigation that considered only area of ice inflow (rather than volume), calculated that 73% of the total yearly ice import occurs during the months

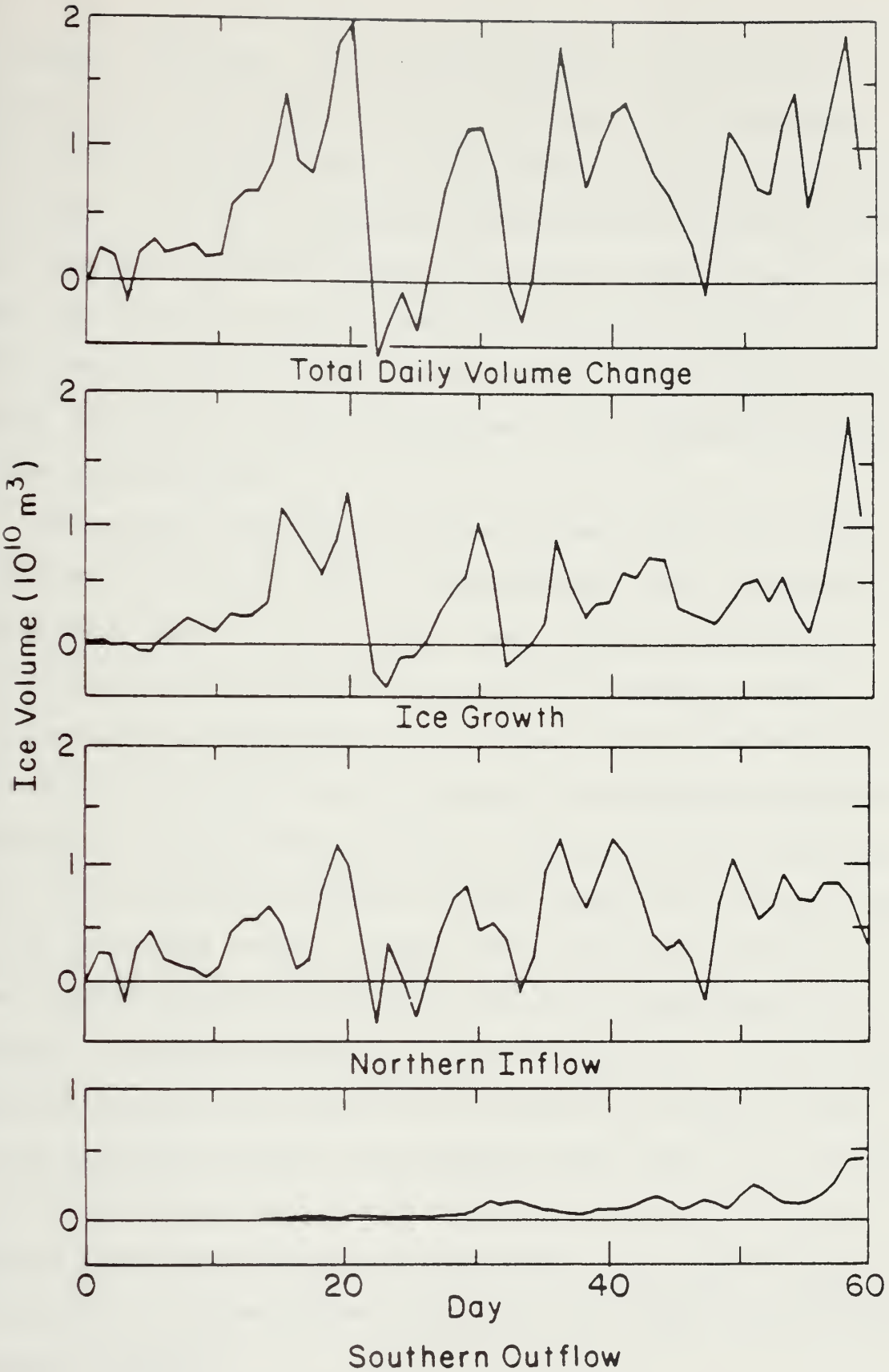

Figure 10. Simulated daily changes in total ice volume and daily volumes of growth, northern inflow and southern outflow.

of December through May. This large rate was due to the increased northerly winds that typically occur during winter. His calculations further showed that only 11% of the total inflow took place during October and November. If this is indeed the normal case, then the yearly inflow that the model would predict would be $4.3 \cdot 10^{12}$ m^3. This value is 36% higher than Aagaard's estimate. Because these are only estimates of inflow, however, it is difficult to assess the validity of the simulated inflow. The simulated value at least seems to be of reasonable magnitude for the two-month period.

The simulation predicts the total ice volume increase to be $7.85 \cdot 10^{11}$ m^3 for the two-month period. This constitutes a 99% increase over the initial amount of ice. Of this total volume, 49.6% was contributed by inflow (with southern outflow removed) and 50.4% was added by growth. That inflow and growth produced nearly equal volumes of ice is somewhat surprising. The suspicion that too much ice growth is taking place is somewhat confirmed by once again comparing relative results to those of Einarsson (1972). In attempting to establish an annual budget for the region between 76°N and the Denmark Strait, the region where most of the predicted ice growth takes place, he estimates that ice growth is approximately 1/4 of the inflow at 76°N for the months of October and November. In this region, the growth-to-inflow ratio predicted by the model is at least as high as that for the entire grid area. The predicted ratio, which is 1:1, combined with an ice inflow rate that appears reasonable, indicates that far more growth is taking place than Einarsson estimated. Once again, it appears that the lack of a proper parameterization of oceanic heat flux is allowing excessive ice growth.

The accuracy of the predicted ice velocities at particular locations can be assessed by comparing them to the velocities of buoys that were drifting on ice floes during this time period. The trajectories of ICEX buoys 1564 and 1568 (Kloster and Rafto, 1980) are shown in Figure 11. An interesting feature of the trajectories is that buoy 1568, which is located some 50 to 140 km closer to the ice edge, showed a much larger displacement in an overall shorter time period (8 days less) than did buoy 1564. It is also apparent that the speed of both buoys increases southward. Vinje (1972, 1973, 1981) and Wadhams (1981) have previously reported on an acceleration of ice as distance southward and distance from the coast increase.

To compare predicted velocities with those of the buoys, daily velocities were interpolated from the grid for the appropriate buoy location. The predicted and observed u and v components of velocity are shown in Figures 12 and 13. Both predicted and observed velocities show high frequency components which can be attributed to the fluctuating winds. It appears that the predictions for buoy 1564 are superior to those for buoy 1568. Additionally, the v components of both buoys seem better predicted than the u components. Correlation coefficients between predicted and observed u and v components are 0.48 and 0.57, respectively, for buoy 1564, and 0.36 and 0.56 for buoy 1568. Because the means are removed when calculating correlation coefficients, this is an effective test of the ability of the model to predict only the high frequency components of the buoy velocities. This is demonstrated by the high correlation coefficient obtained for the v component of buoy 1568, where, in fact, large differences between the velocity magnitudes are apparent. These differences become clear when comparing predicted and observed means for buoy 1568

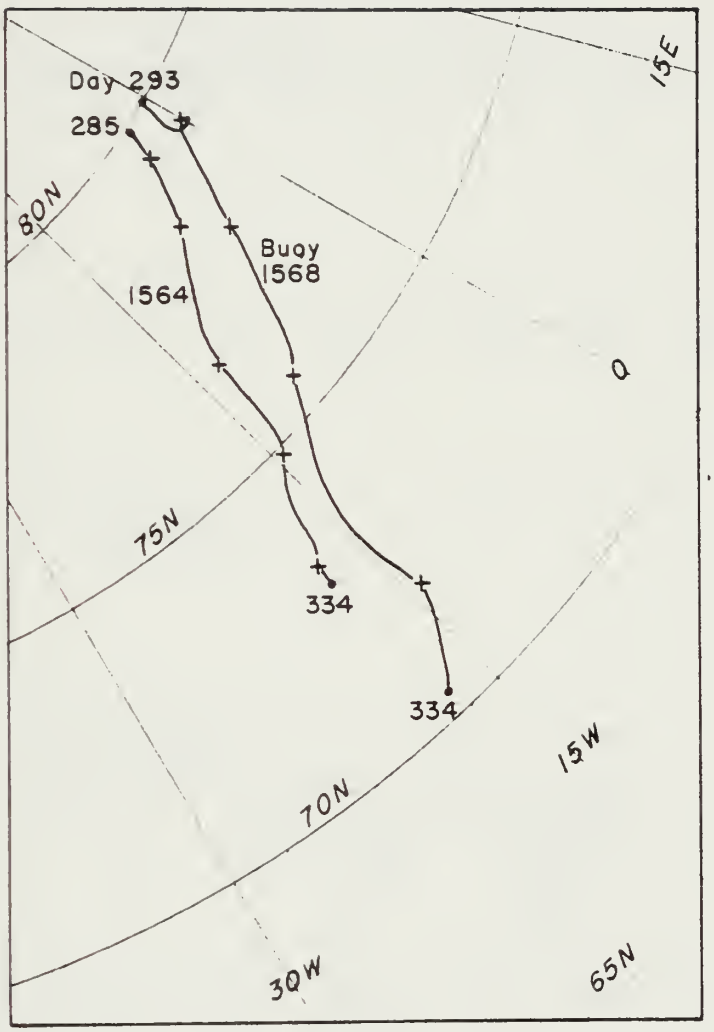

Figure 11. Trajectories of ICEX buoys 1564 and 1568.

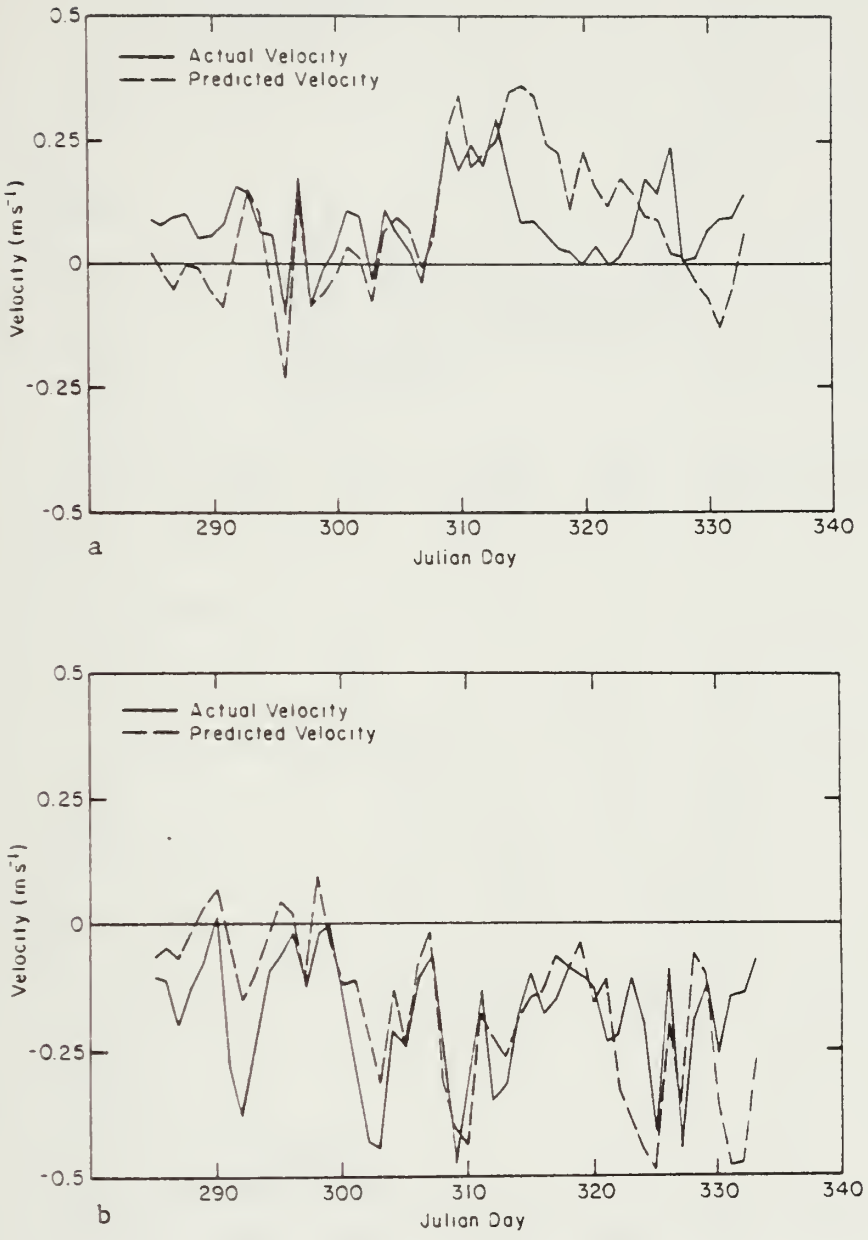

Figure 12. Observed and predicted components of velocity for ICEX buoy no. 1564.
a) u component.
b) v component.

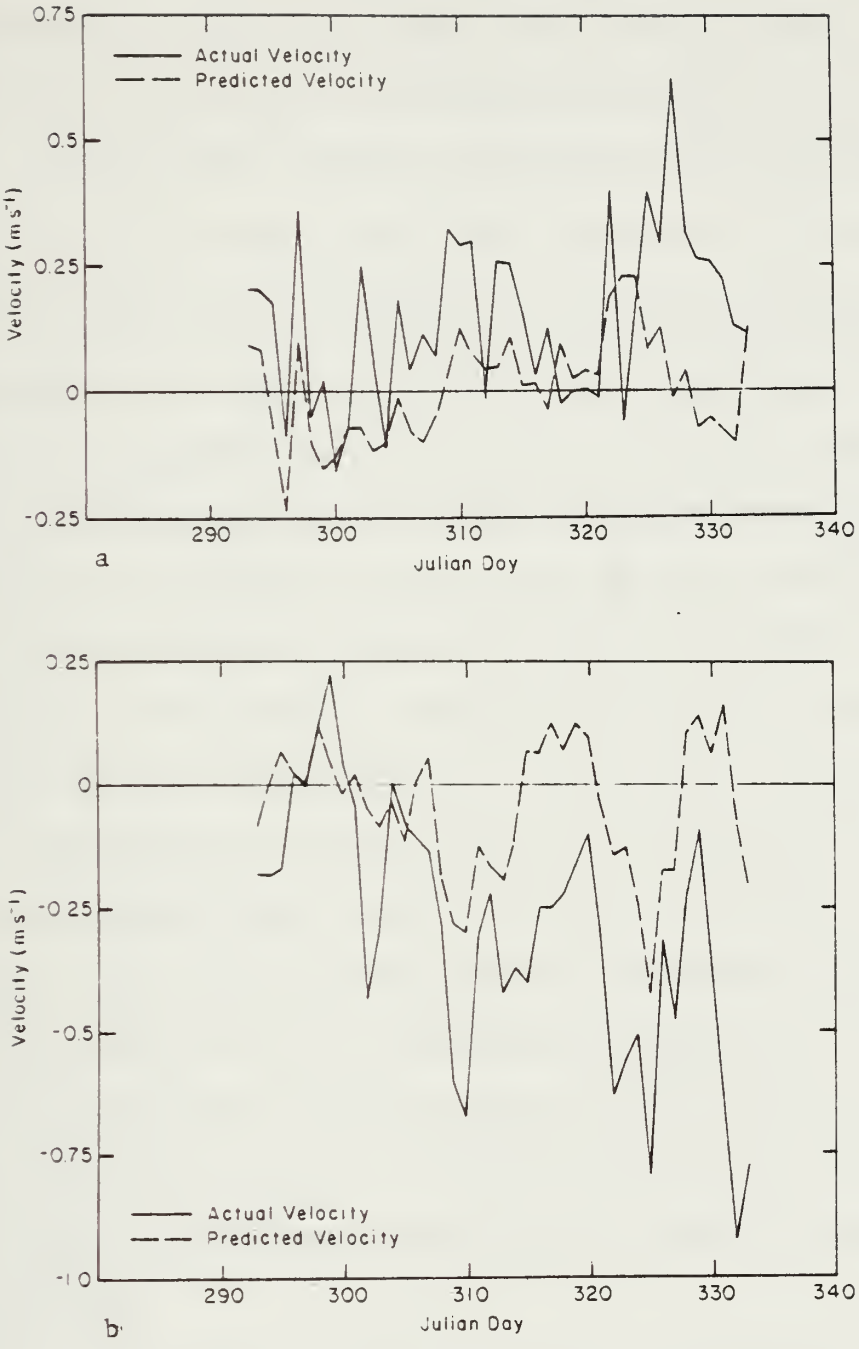

Figure 13. Observed and predicted components of velocity for ICEX buoy no. 1568.
a) u component.
b) v component.

velocities. The predicted u and v velocity means are 0.01 and -0.04 m s^{-1} respectively, while those for the actual velocities are 0.15 and -0.30 m s^{-1}. In contrast, the u and v predicted velocity means for buoy 1564 are 0.08 and -0.17 m s^{-1} and those of the observed velocities are 0.08 and -0.19 m s^{-1}. Another useful statistic for assessing the predictability of the velocities is the Root Mean Square error $\left(\text{RMS error} = \left[\frac{1}{N}\sum (\text{Predicted-Observed})^2\right]^{1/2}\right)$ which gives some feeling for the error of amplitude for an individual velocity. The RMS errors for the u and v velocities were 0.12 and 0.14 m s^{-1} for buoy 1564 and 0.21 and 0.33 m s^{-1} for buoy 1568. Comparison of the correlation coefficients, velocity means and RMS errors rapidly verifies, as do Figures 12 and 13, that the daily velocities of buoy 1564 are more accurately simulated than those of buoy 1568.

The accuracy of the simulated velocity field can also be assessed by calculating the simulated trajectories of the two buoys. The trajectory is computed by interpolating a predicted velocity for the predicted buoy position of the previous time step, using the initial buoy position for a starting point. The trajectories for both buoys are shown in Figure 14. The simulated trajectories are not satisfying, particularly for buoy 1568. In this case the calculated trajectory placed the buoy within the boundary region where velocities are zero. The simulated trajectory for buoy 1564 is somewhat better but its "miss distance" for the final buoy position (day 334) is quite large.

Simulated trajectories are quite sensitive to the time and place chosen for the buoy's initial point. To demonstrate, the extremely poor case of buoy 1568 can be somewhat improved by starting the buoy at a later

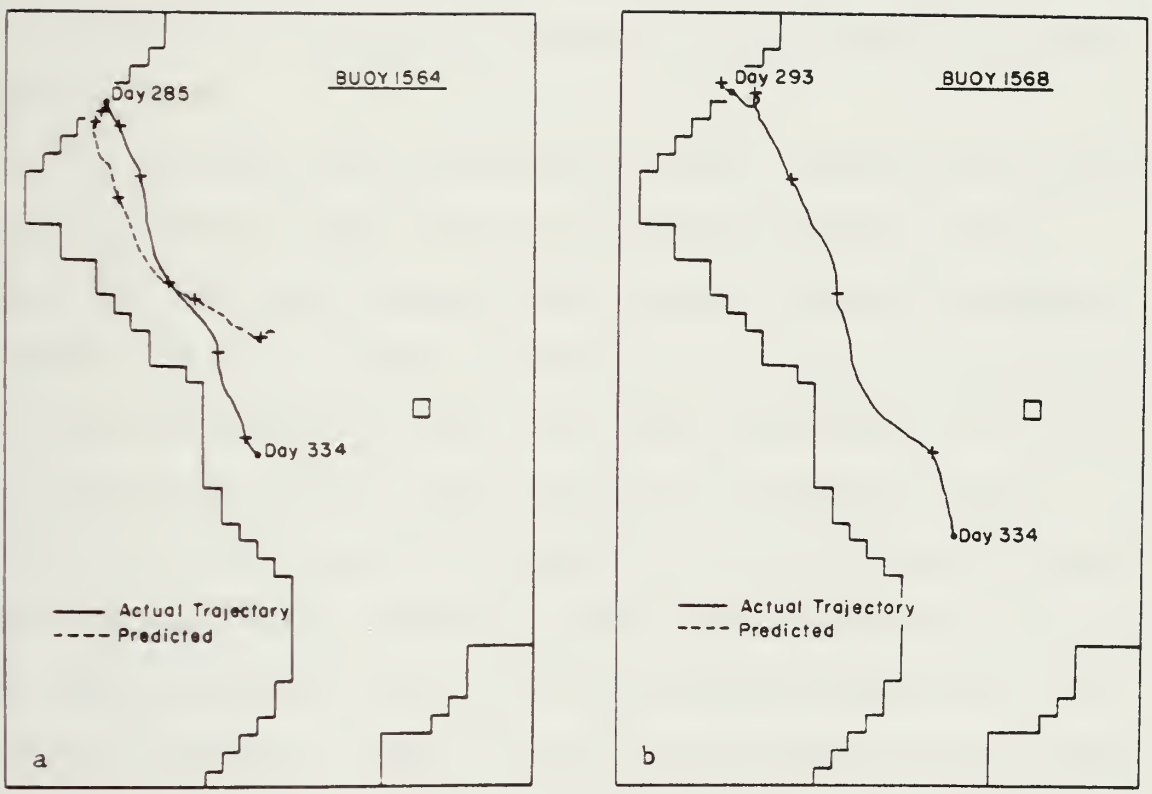

Figure 14. a) Predicted trajectory for buoy 1564.
b) Predicted trajectory for buoy 1568.
Crosses indicate 10 day Julian day intervals (i.e. 300, 310..,).

time and by choosing a different starting location. Figure 15a shows a simulated trajectory obtained by starting the buoy 4 days later while in Figure 15b the starting day is the original day (293) but its starting location has been moved approximately 90 km west. Although the simulated trajectories are still not acceptable, significant improvement has taken place over the original trajectory shown in Figure 14b. The point to be made here is that small errors in the predicted velocity field over only a few days, or uncertainty in the actual buoy starting location, can result in a totally unrealistic trajectory. This can easily lead to the belief that velocities in the region of the buoy are unrealistic for the total trajectory period.

While the above method calculates an "ideal" trajectory, the results are very sensitive to small errors in the simulated velocity field or initial buoy location as has been shown. Another method of computing a trajectory, which is not quite so sensitive, is to again sum the predicted daily velocities, only this time to take these velocities from the actual daily position of the buoy, rather than from the predicted position. In essence, this method consists of summing the predicted velocities shown in Figures 12 and 13. This technique is quite useful for examining the long term cumulative effects (and errors) of the predicted velocities at the locations of the buoys. Figure 16 shows the trajectories for both buoys calculated in this manner. Once again it becomes clear that the velocities predicted for buoy 1564 were far superior to those of buoy 1568. What is made particularly obvious in this figure is that the v velocity components simulated for buoy 1568 are significantly in error, as can also be clearly seen from Figure 13.

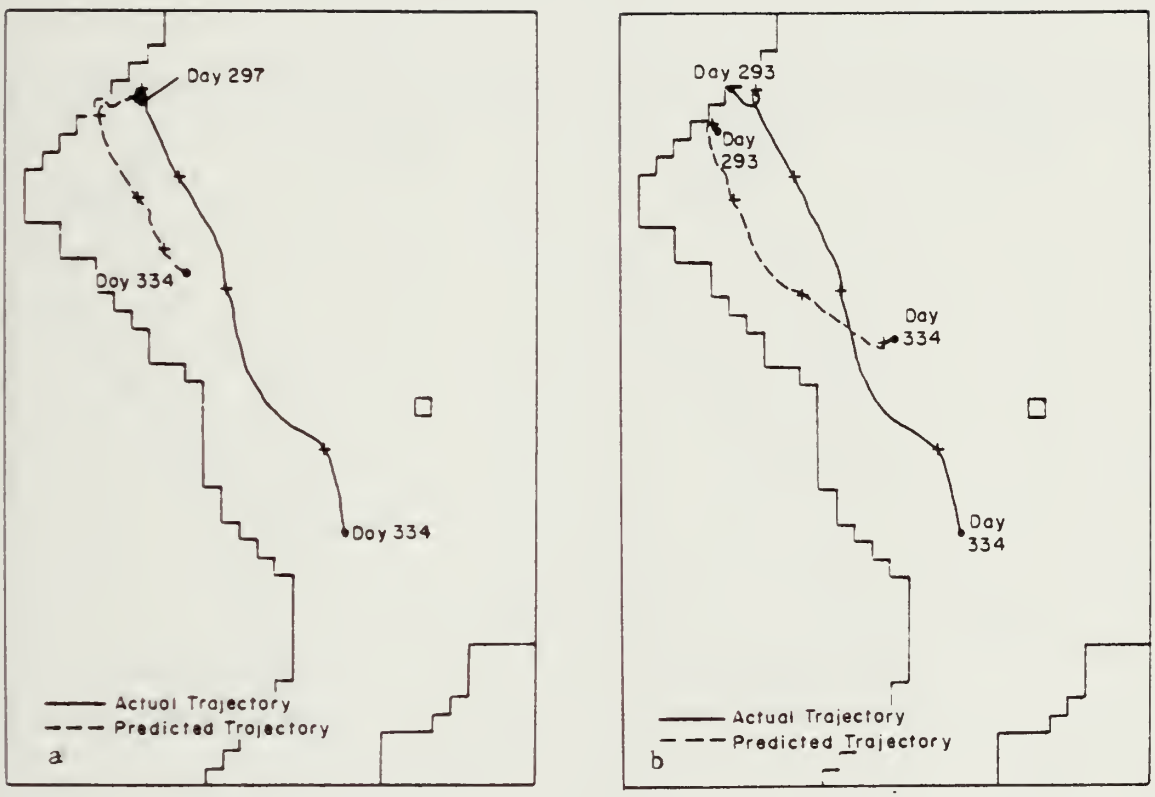

Figure 15. Predicted trajectories for buoy 1568:
a) beginning on day 297.
b) simulating the starting position 90 km to the west of the actual starting location.

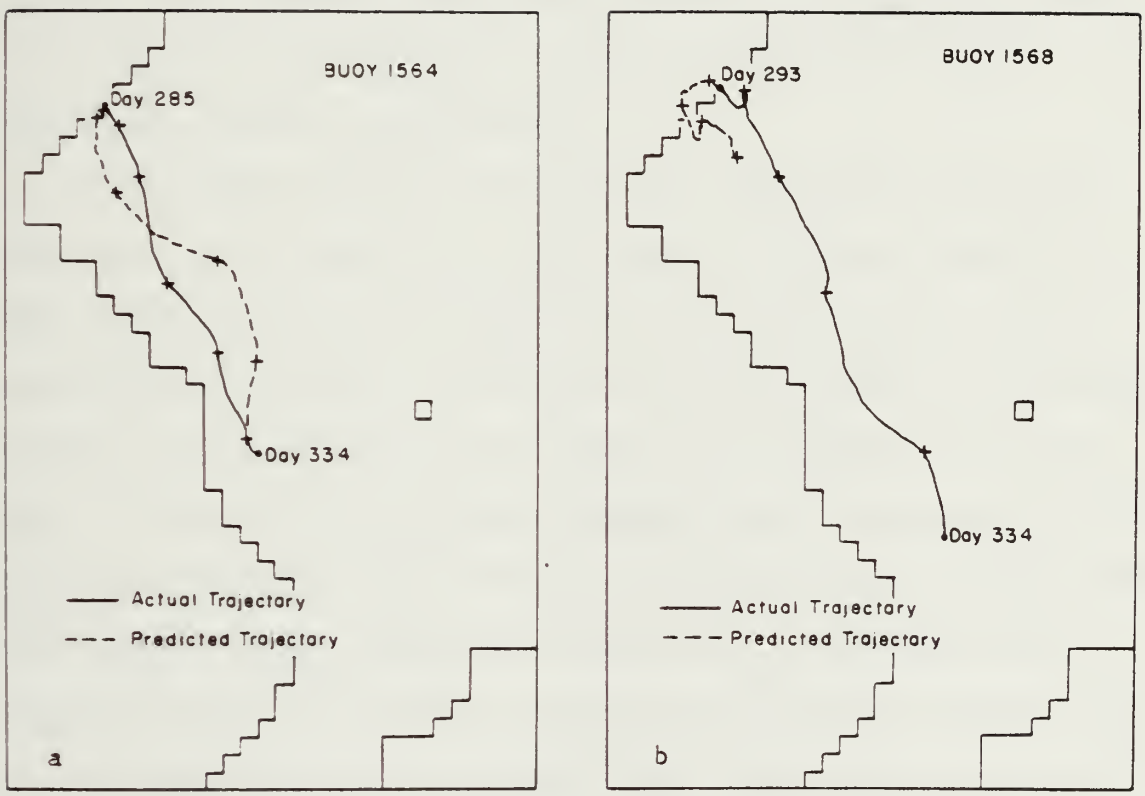

Figure 16. a) Cumulative daily predicted trajectory for buoy 1564.
b) Cumulative daily predicted trajectory for buoy 1568.

The behavior of these trajectories can be analyzed in detail using the 10-day averaged velocity fields (Fig. 7 a-f); however, the 60-day averaged velocity field can be used for a brief summary. For descriptive purposes, the actual buoy trajectories are shown superimposed on the simulated 60-day averaged ice velocity field in Figure 17. The trajectory of buoy 1564 placed it nearer the simulated high ice velocity stream adjacent to the Greenland coast, which allowed its predicted trajectories (by either method) to advect it southward. The predictions of buoy 1568 were less fortunate. Its starting position (and subsequent positions) placed it to the east of this predicted high velocity region. It is for this reason that the excercise which moved its starting location 90 km west significantly improved the trajectory.

The surprising feature of the predicted trajectories is that the poorest predictions were for buoy 1568, which in actuality showed the largest displacement and far higher velocities than buoy 1564. This results from the fact that the predicted velocities closer to the ice edge were poor. One major problem here appears to be related to the wind fields. A comparison of the 60-day averaged winds (Fig. 3a) and the 60-day averaged ice velocities (Fig. 7g) leads to the belief that the high velocity ice stream is highly dominated by the winds. As a result, the ice velocities fall off too rapidly to the east, and the high velocities that apparently existed near the ice margin during this period are not properly accounted for.

Other processes may also have been responsible for the observed acceleration of the ice near the edge. Mesoscale oceanographic or meteorological phenomena associated with the ice edge could conceivably cause

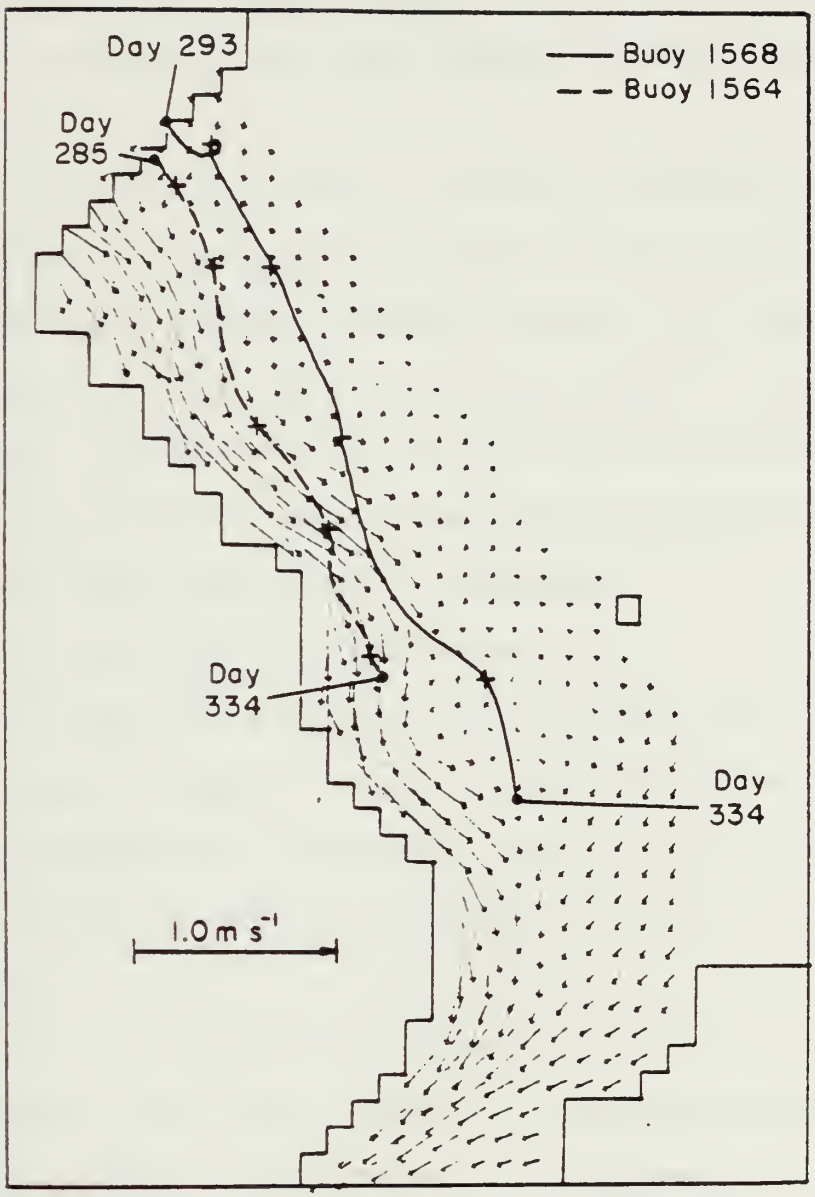

Figure 17. Actual buoy trajectories superimposed on the 60-day averaged ice velocity field.

density currents or winds that would not be resolvable in synoptic scale data. In particular, mesoscale winds resulting from local baroclinicity or katabatic effects may be occurring here. Also, temporally varying oceanic processes would not be accounted for by the climatological dynamic height field used to calculate the geostrophic currents that were used in this study.

Another possible scenario which may cause an acceleration of ice near the edge has recently been suggested by Roed and O'Brien (1981). In this work, an analysis of a dispersive medium is carried out in which a momentum equation included a pressure term. This pressure term is directed normal to the ice edge, and presumably could result from the random bumping of ice floes. After geostrophic adjustment, the velocity field exhibits a jet-like structure near the ice edge. A phenomenon of this nature may be the solution to the problem presented here and, if so, could be accounted for by the model used in this study by a modification of the constitutive law in the ice margin region. The first inclination, however, is to carry out a detailed examination of the synoptic wind and current fields used in this study to see if they adequately represent the actual winds or currents in this region.

Because all other simulations provided equally as poor or worse predictions than the standard run for buoy 1568, no further comparisons to this buoy will be made. In addition, when trajectories are calculated, only the cumulative daily trajectory method will be used because it points out all essential features and because the "ideal" trajectories behaved quite poorly on the remaining simulations, being so sensitive to the ice velocities at the initialization time and position.

C. THERMODYNAMIC SIMULATION

For this simulation, only the growth rates calculated for the region were of concern. This sensitivity test was carried out simply by setting all ice velocities to zero in the numerical code. In this manner, thickness, concentration and ice extent can increase (or decrease) only according to the growth rates derived from the thermodynamic code.

Figure 18 presents the thickness and compactness fields as predicted by the model at the end of the 60-day simulation period. This figure shows that the ice extent has increased significantly over the initial field (Figs. 5a and 6a). The expansion has taken place almost entirely due to growth of thin ice, however. The thicker ice ($\geq$ 1.0 m) has expanded very little, a good indication of the significant difference in the growth rates between thick ice and thin ice/open water.

Comparison of the thickness and compactness fields of the thermodynamic simulation (Fig. 18) to those of the 60-day thickness and compactness predicted by the standard run (Figs. 5g and 6g) gives some perception of the effects of ice dynamics. The most obvious difference is that much more thick ice occurs near the coast in the complete simulation, a result of dynamically induced advection and subsequent ridging of ice of all thicknesses. The effects of divergence which created the lower concentration areas, both along the coast and elsewhere, are also not apparent in the compactness field produced by the thermodynamic simulation.

The position of the ice edge relative to the reported edge position, also shown in Figure 18, shows little improvement over that predicted by the standard run. This tends to confirm suspicions expressed earlier that the ice growth rates were responsible for the excessive ice extent. This

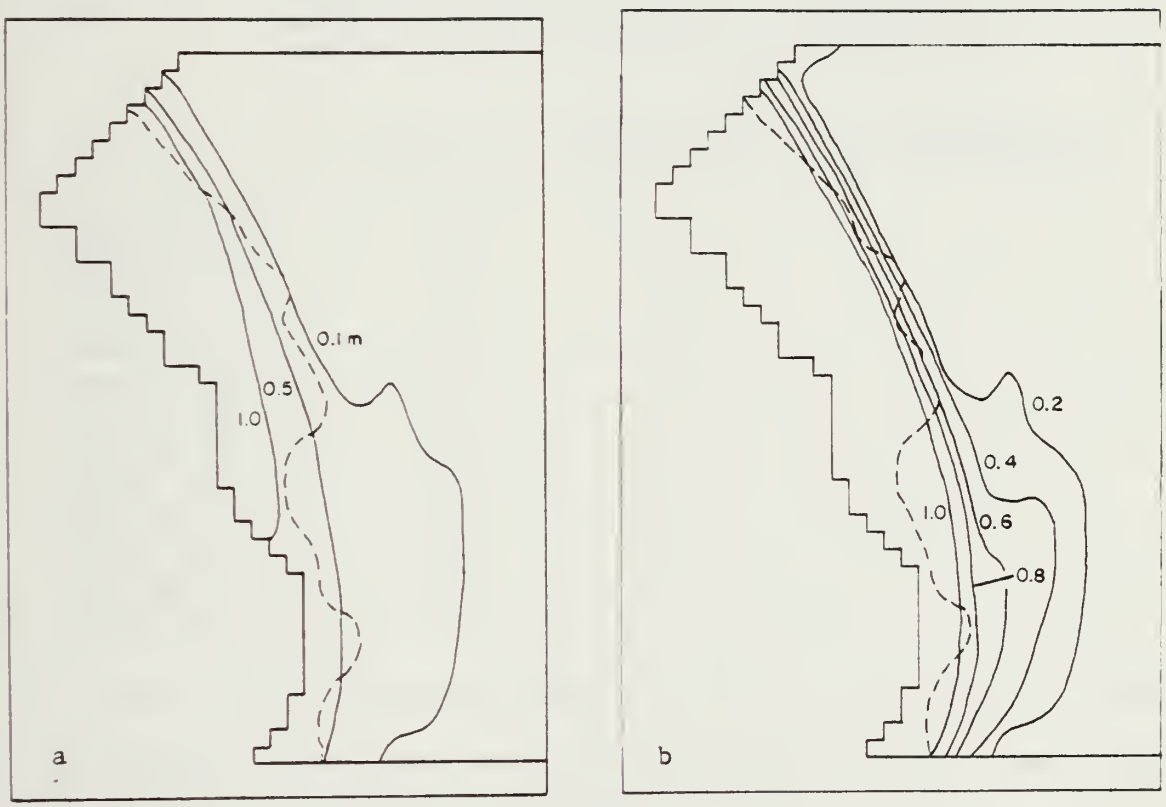

Figure 18. a) 60-day thickness field for the thermodynamic simulation. b) 60-day compactness field for the thermodynamic simulation. Dashed line is observed ice edge position for 2 December 1979 (NPOC, 1979).

is particularly applicable to the southern section of the grid where the largest expansion has taken place. To examine the areal extent of ice in more detail, it is useful to prepare a table similar to Table I. Table II presents the area of ice coverage at 10-day intervals along with the percentage increase during the intervals. In addition, the percent difference in coverage between the thermodynamic simulation and both the reported coverage and that generated by the standard run are included.

Table II. Predicted areas (in 10^{11} m^2) of ice cover for the thermodynamic simulation for 10 day intervals with the percent difference between this simulation and the observed coverage and the standard simulation.

	Predicted	% Difference from Observed	% Difference from Standard Run
Initial Area	1.80		
Area Day 10	1.82	-17.6	- 3.2
Change (%)	1.1		
Area Day 20	3.51	56.7	- 1.1
Change (%)	92.8		
Area Day 30	3.56	72.8	5.3
Change (%)	1.4		
Area Day 40	3.85	65.2	1.5
Change (%)	8.1		
Area Day 50	4.26	71.8	- 5.4
Change (%)	10.6		
Area Day 60	5.56	77.6	- 4.8
Change (%)	30.5		

The table clearly shows that differences of areal ice coverage between the thermodynamic and standard simulations are small. In some cases (days 30 and 40), it appears that the ice dynamics of the standard run were acting to restrain the ice extent. At all times, however, the differences are small enough that the excessive ice extent can be attributed almost entirely to thermodynamic growth. Both the predicted percentage changes during the 10-day intervals and the percent difference from the observed extent are similar to those of the standard run.

That the thermodynamics are dominating the ice extent and edge location in these simulations should not be construed to imply that ice dynamics are not relevant to this process. A judgment of this nature would be premature at this point. The problem at hand, as has been mentioned several times previously, is that the present growth rates seem to be excessive. This, in turn, so dominates the simulated ice extent that the effective role of dynamics in determining ice extent appears to be small. The actual role of the ice dynamics in this process will not be properly resolved until more realistic ice growth rates are utilized.

The total volume of ice produced in the thermodynamic simulation is much less than that produced in the standard run. The volume change here was $2.57 \cdot 10^{11}$ m^3 compared to $7.85 \cdot 10^{11}$ m^3 for the previous simulation. In this simulation, growth accounted for all the volume change, while in the standard run it accounted for approximately half of the change, that being $3.95 \cdot 10^{11}$ m^3. The standard run, then, produced 53% more ice by growth than the thermodynamic simulation. This increase in growth due to the dynamics is likely due to new ice growth in areas of dynamically induced ice divergence. The salient point here is that the ice dynamics actually increases ice production by thermodynamics. Similar results were found by Hibler (1979) in a modeling study of the Arctic Basin. This result could be very significant to studies dealing with air-sea heat exchange in this region. The implication is that such studies must include the effects of ice dynamics to properly treat air-sea energy exchanges.

D. ZERO ICE STRENGTH

The effect of the internal ice stress term in the momentum balance can be assessed by allowing the ice to have no strength. This damps out ice

interaction with itself and effectively creates a free drift situation. With the zero strength condition imposed, the ice also has no resistance to deformation. In practice, this case is simulated by setting P*, an empirical constant in equation (4), to zero. This effectively results in the ice strength and bulk and shear viscosity terms all being zero, thus eliminating the internal ice stress term, F, in equation (1).

Thickness and compactness fields at the end of the 60-day simulation period are shown in Figure 19. A salient characteristic of the zero strength condition is manifested by the unreasonably large thickness build-ups that have occurred adjacent to the coast. The necessity of allowing the ice to interact with itself in any effort to model this region is clearly demonstrated by this figure. Farther east, nearer the ice edge, thicknesses appear to be more reasonable; thus it seems that a free drift model may perform adequately here.

The 60-day averaged velocity field for the zero strength simulation, shown in Figure 20, helps explain some of the features apparent in the thickness and compactness fields. A definite onshore velocity component is obvious in several locations along the coast. This onshore component, which is a result of strength being independent of thickness (actually zero in this case), amplifies the effect created by the ice having no resistance to deformation and results in the physically unrealistic thicknesses. Comparison of this velocity field to that of the standard run (Fig. 7g) manifests the rectifying effect that ice interaction allows. Higher ice stresses near the coast in the standard run effectively curtail further motion in that direction, yet allow motion toward areas of less stress.

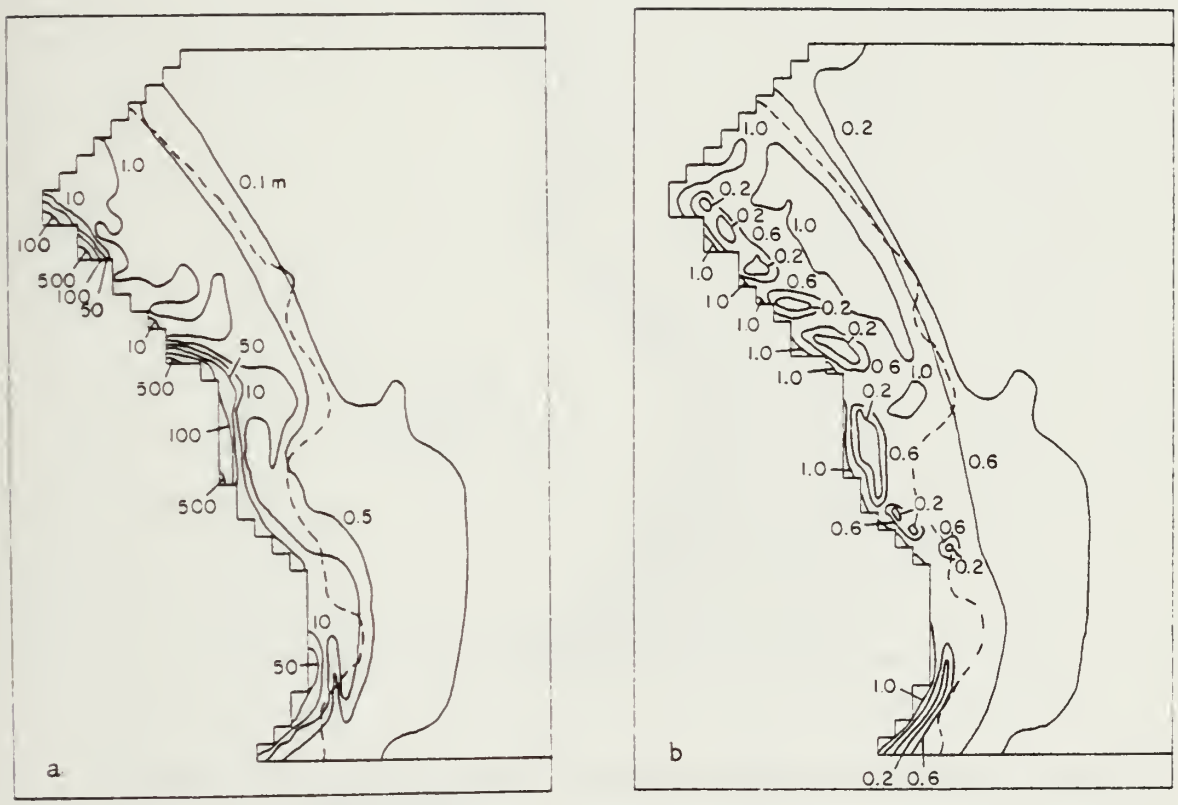

Figure 19. a) 60-day thickness field for the zero strength simulation. b) 60-day compactness field for the zero strength simulation. Dashed line is observed ice edge position for 2 December 1979 (NPOC, 1979).

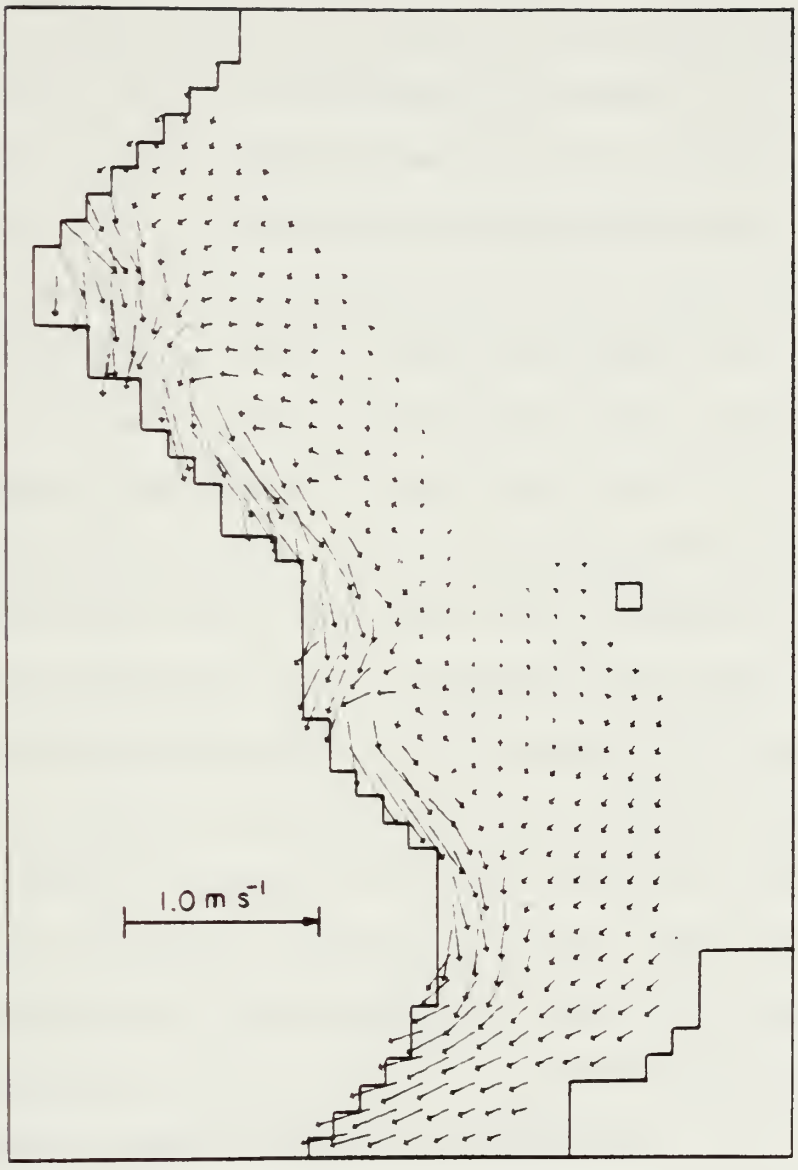

Figure 20. 60-day averaged velocity field for the zero strength simulation.

The compactness "holes" which appear short distances away from the coast are also created by the ice dynamics. Here, ice is simply being advected away from a particular area faster than it can be replaced by advection from an adjacent area or by growth. This results in the creation of low concentration cells. The phenomenon is prevented in the standard simulation because velocity magnitudes near the coast are decreased by higher strengths. With these numerous low concentration areas, it is not surprising that the area of ice coverage at the end of the simulation is $4.47 \cdot 10^{11}$ m^2, a value that is 23% less than the standard run.

The total ice growth for this simulation was $1.55 \cdot 10^{13}$ m^3, a value that is two orders of magnitude higher than that of either the standard run or the thermodynamic simulations. This unreasonably high value is presumably due to the growth of ice in the areas of ice divergence. The reasoning here is that if nearly all the ice is advected out of these areas (the low compactness cells) at every time step, the high growth rates of thin ice and open water will be continually sustained, leading to excessively high total ice growth. In contrast, the total inflow for the period appears to be more reasonable, being $6.18 \cdot 10^{11}$ m^3. This is 30% larger than the inflow predicted by the standard run. This is not surprising, however, because higher velocities are to be expected for the inflow region, and these are indeed in evidence in Figure 20.

The correlation coefficients between the predicted and observed velocities of buoy 1564 were 0.45 for both u and v components. These coefficients are less than those of the standard run, particularly with the v component (0.57 for the standard run). The predicted velocity means are -0.03 and -0.17 m s^{-1} for the u and v components (0.08 and -0.19 m s^{-1} for

the observed). The u component mean shows an excessive onshore velocity trend. RMS errors are also higher than those of the standard run, being 0.16 m s^{-1} for both u and v components (0.12 and 0.14 m s^{-1} for the standard run). The true deficiencies in the velocity predictions, however, are made more apparent by the cumulative daily predicted trajectory for buoy 1564, which is shown in Figure 21. The excessive onshore component of velocity is quite evident in this figure, eventually placing the buoy well into the boundary area representing Greenland. Once again, the lack of a velocity rectification effect produced by ice interaction is made clear by the comparison of this trajectory with that of the standard run (Fig. 16a).

E. ZERO ICE IMPORT

Previous simulations have shown that the ice inflow through the Fram Strait constitutes a major part of the mass budget in this region. In this light, a worthwhile sensitivity test is to not allow inflow and assess the impact of this on the model results. Zero inflow is simulated simply by specifying zero thicknesses for the northern free boundary cells.

Figure 22 shows the thickness and compactness fields at the end of the 60-day simulation. These fields are similar to the analogous fields of the standard run (Figs. 5g and 6g), with several notable exceptions. These discrepancies are particularly apparent in the northern section of the grid. The most apparent difference is that thicknesses are generally lower in this section. Coastal build-ups in this region are much less than those produced in the standard simulation. Similar features occur in the compactness field where lower concentrations have developed in the northern section. The southern third of the grid area and the total ice extent are virtually unchanged between the two simulations, however. The cause for

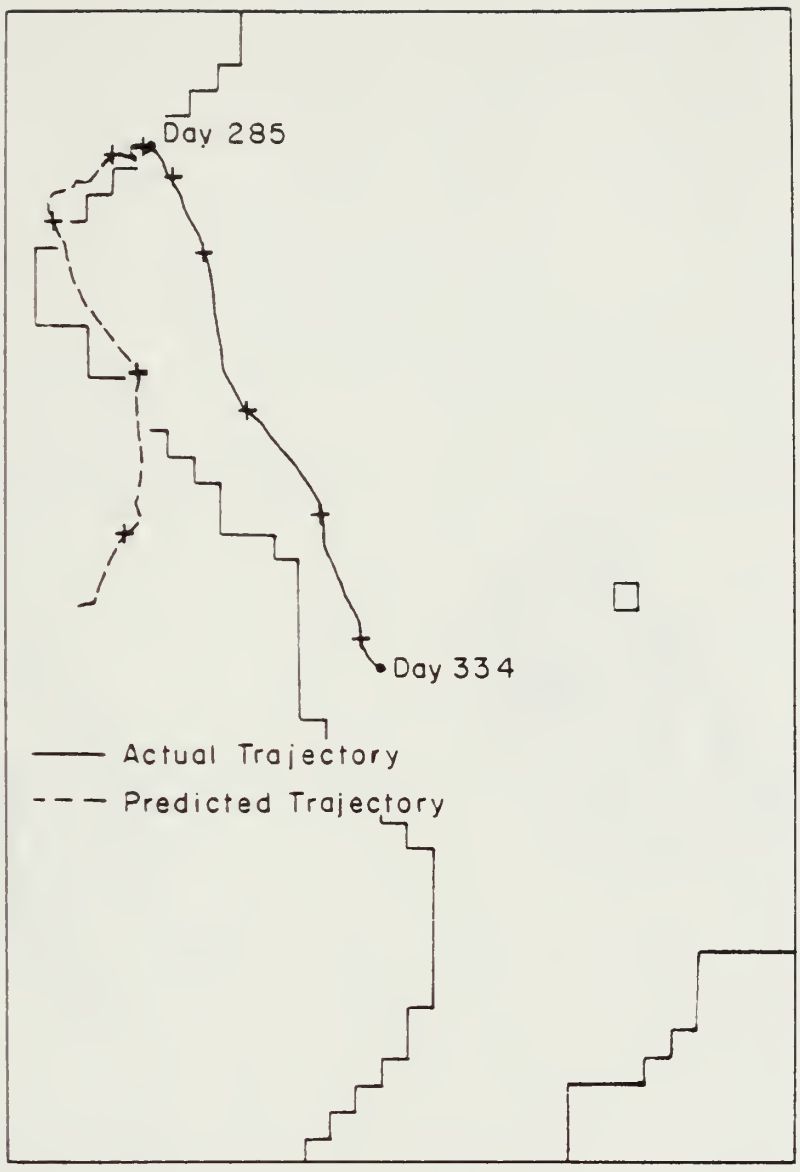

Figure 21. Cumulative daily predicted trajectory for buoy 1564 for the zero strength simulation.

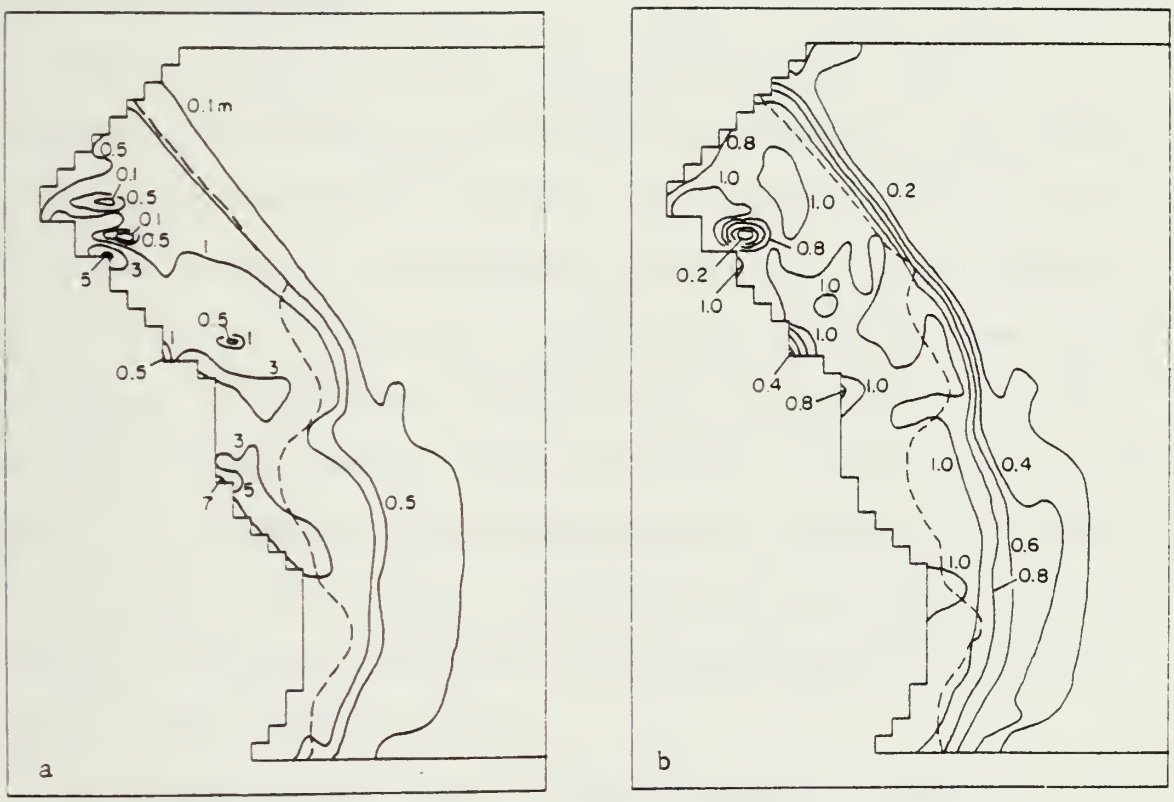

Figure 22. a) 60-day thickness field for the zero inflow simulation. b) 60-day compactness field for the zero inflow simulation. Dashed line is observed ice edge position for 2 December 1979 (NPOC, 1979).

these differences in the northern sector is obviously that ice is being transported southward or ridged near the coast, and no thicker ice is being advected in through the free boundary to replace it. Also, new ice growth is not sufficient to sustain the 100% concentration level in this high velocity region. However, the growth of thin ice is occurring at a relatively high rate due to the advection of ice out of the northern region. The total ice growth for this simulation was $5.62 \cdot 10^{11}$ m^3, a 40% increase over the standard run. Because velocities are less near the ice edge, its position is predominantly controlled by thermodynamics, as was the case for the standard simulation.

That the southern region of the simulation area is free from the effects of no inflow during this simulation is verified by the volume of ice exiting the southern open boundary. For both the standard run and the zero inflow cases, the total southern outflow volume for the 60 days is $0.83 \cdot 10^{11}$ m^3. The implication is that during this period, the effects of "running out" of thick ice, as has occurred in the north, had not yet reached the southern outflow region. This fact is obvious from the similarity of the thickness and compactness fields to those of the standard run in the southern region. The indication is that the southern region would eventually be affected, but an appreciably longer simulation would be required to sort out these effects.

The 60-day averaged velocity field is presented in Figure 23. With the exception of the northern region, where velocities have a slightly greater onshore component, the velocities are nearly identical with those of the standard run (Fig. 7g). The larger onshore component and slightly higher magnitudes can be attributed to lower ice strengths in the region.

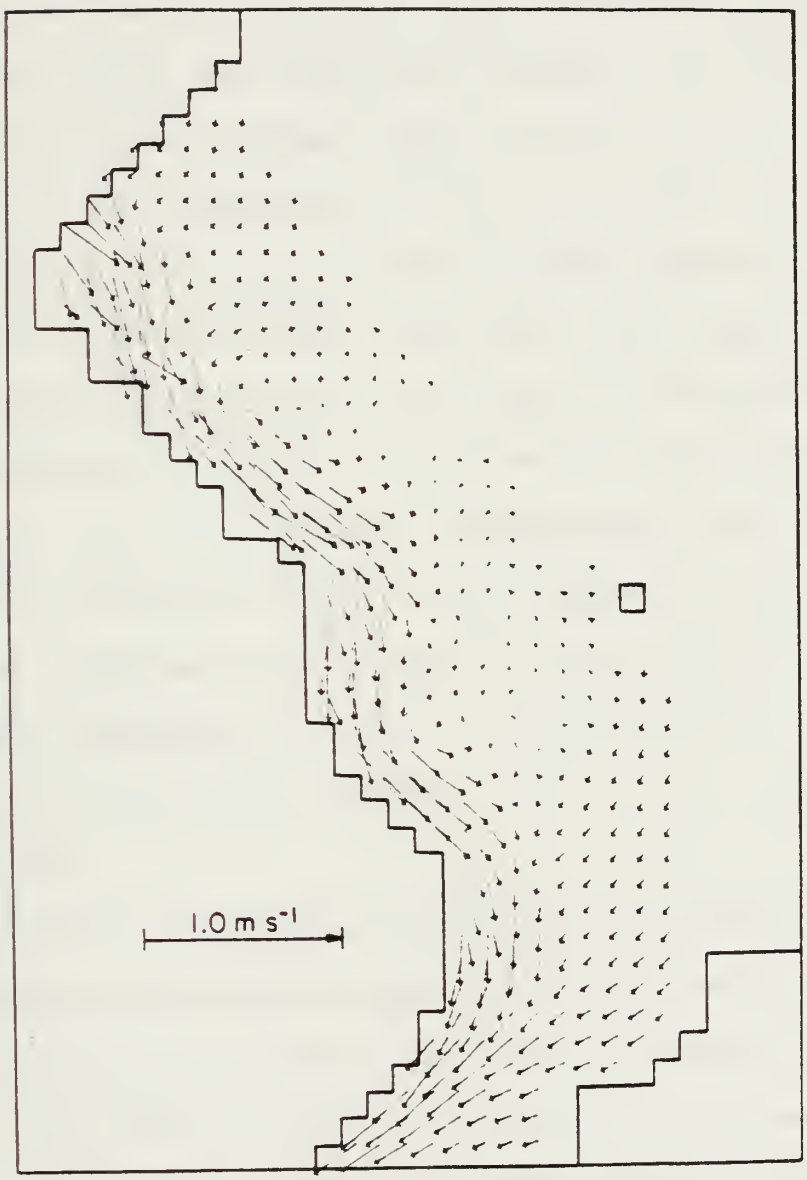

Figure 23. 60-day averaged velocity field for the zero inflow simulation.

Here lower strengths have again been induced by the lower ice thicknesses and concentrations.

Correlation coefficients of the u and v velocity components with those of buoy 1564 are 0.48 and 0.52, respectively. The v coefficient is only slightly less than that of the standard run (0.57). The predicted velocity means are 0.06 and -0.16 m s^{-1} for the u and v components — only slightly different from those of the standard run (0.08 and -0.19 m s^{-1}). RMS errors for the predicted components are 0.14 and 0.15 m s^{-1}, once again, close to those of the standard run (0.12 and 0.14 m s^{-1}). The cumulative daily predicted trajectory for this buoy is shown in Figure 24. The slight onshore velocity component is again emphasized in this figure, with the buoy being placed slightly closer to shore than with the standard simulation. The trajectory in this case also misses the final buoy position by a larger distance than the standard run, bearing out the lower correlation coefficient and less negative mean for the v component. Overall, however, the velocities do not seem greatly affected by the zero inflow stipulation. A longer simulation, in which thicknesses decreased over the entire region, might show significant effects.

F. ZERO CURRENTS

This sensitivity test examines the effect of the geostrophic currents specified for the other simulations simply by turning those currents off. With this specification, the ice can be thought of as moving across a stagnant ocean. Water stress is still an integral part of the momentum equation, only it is calculated with a zero current velocity. The force due to the tilt of the sea surface is also zero in this case.

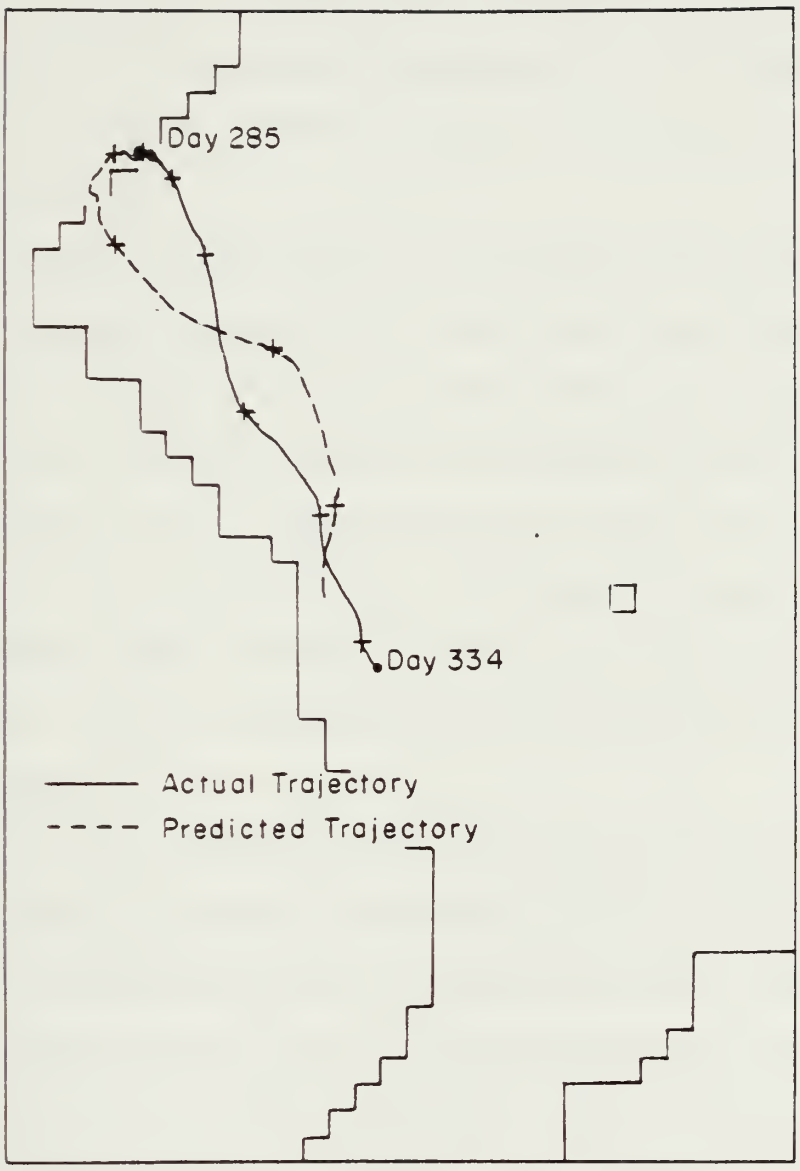

Figure 24. Cumulative daily predicted trajectory for buoy 1564 for the zero inflow simulation.

At the end of the 60-day simulation period, the thickness and compactness fields were nearly identical to those of the standard run; thus they are not shown here. Even regions of coastal build-ups and low concentrations had approximately the same thickness and compactness values. This is indicative of the nearly negligible effect exhibited by the geostrophic currents specified for the previous simulations on the ice dynamics. The inference is that the ice dynamics in previous simulations has been primarily wind-driven.

With such obvious similarities in the thickness and compactness fields, it is not surprising that the total area of ice coverage at the end of 60 days is $5.78 \cdot 10^{11}$ m^2. This is within 10% of the value predicted by the standard run. The total volume of ice exiting the southern boundary is also quite similar to that of the standard run, being $0.81 \cdot 10^{11}$ m^3 ($0.83 \cdot 10^{11}$ m^3 for the standard run). Differences are apparent in the volume of northern inflow, however. In the zero current simulation that volume is $3.85 \cdot 10^{11}$ m^3, approximately 20% less than the inflow of the standard simulation.

The differences in the volume of northern inflow ice can be attributed to the relatively high current velocities in the inflow area, as shown in Figure 3b. This region would then be expected to be more severely influenced when currents are set to zero. This is manifested by the 60-day averaged ice velocities, shown in Figure 25. Here, velocities of ice entering the grid are shown to be slightly less than those of the analogous figure for the standard run (Fig. 7g). In addition, this field, which is essentially the result of dynamics driven primarily by wind, shows a small velocity component that would drive ice out of this boundary, thus further

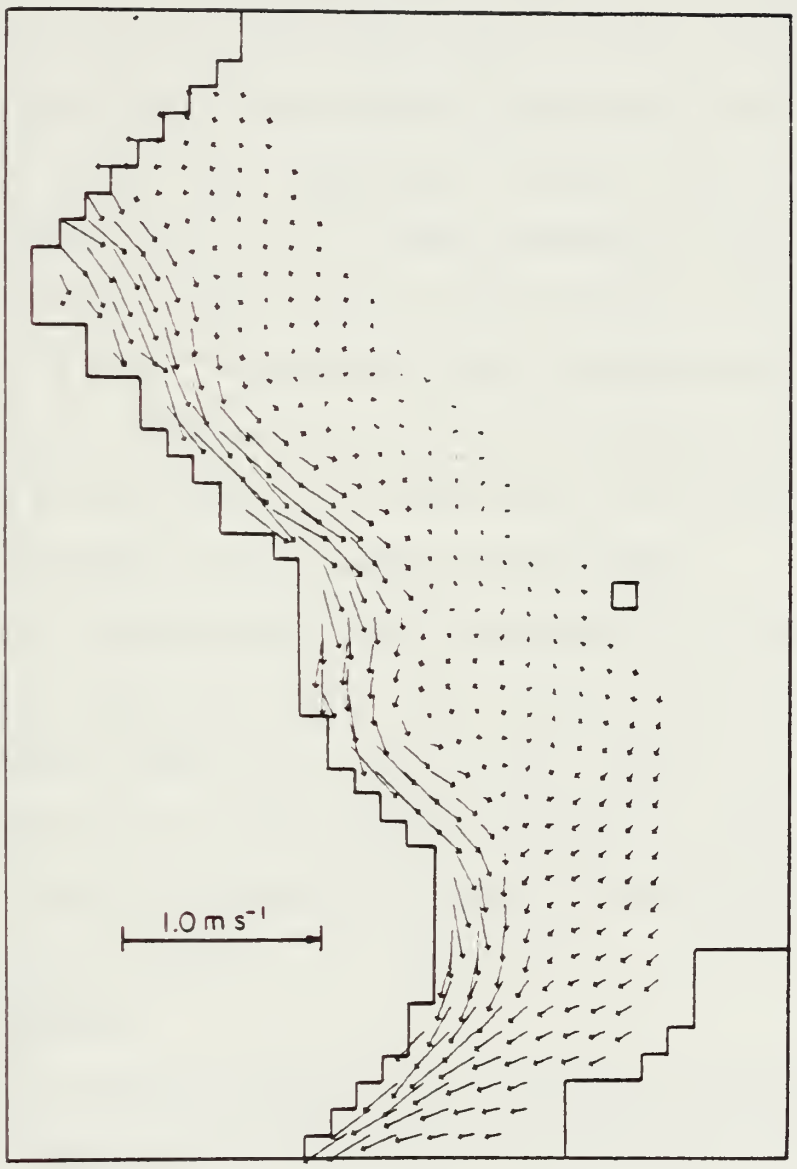

Figure 25. 60-day averaged ice velocities for the zero current simulation.

reducing the net inflow volume. Further south, the velocity vectors appear to be identical to those of the standard simulation.

In further assessment of predicted ice velocities, the correlation coefficients of the u and v velocity components with those of buoy 1564 are 0.47 and 0.54. As with other simulations, these are quite similar to those of the standard run, only being slightly smaller in the v component. The RMS errors are exactly the same as those of the standard run, being 0.12 and 0.14 m s^{-1} for the u and v components. The mean u and v velocity components, 0.07 and -0.15 m s^{-1}, are again comparable to the observed means (0.08 and -0.19 m s^{-1}), and quite close to those of the standard run (0.08 and -0.17 m s^{-1}). The cumulative daily predicted buoy trajectory is shown in Figure 26. The predicted trajectory is slightly further west than that predicted by the standard run, probably due to the greater onshore component of velocities near the northern inflow region.

In general, the geostrophic currents specified for the other simulations had little effect on the model results except at the inflow region. The most significant effect was to increase the volume of ice entering the region by contributing to larger southward velocities. Thicknesses and concentrations over the remainder of the grid seem unaffected by turning off the geostrophic currents.

G. MODIFIED CURRENTS

Because the previous simulation showed that the geostrophic currents had so little impact on the model results, it was decided to dramatically alter the current field. This step was taken partially because previous investigators have attributed a major component of the ice transport in this region to currents (Vowinckel, 1964; Einarsson, 1972). This study is

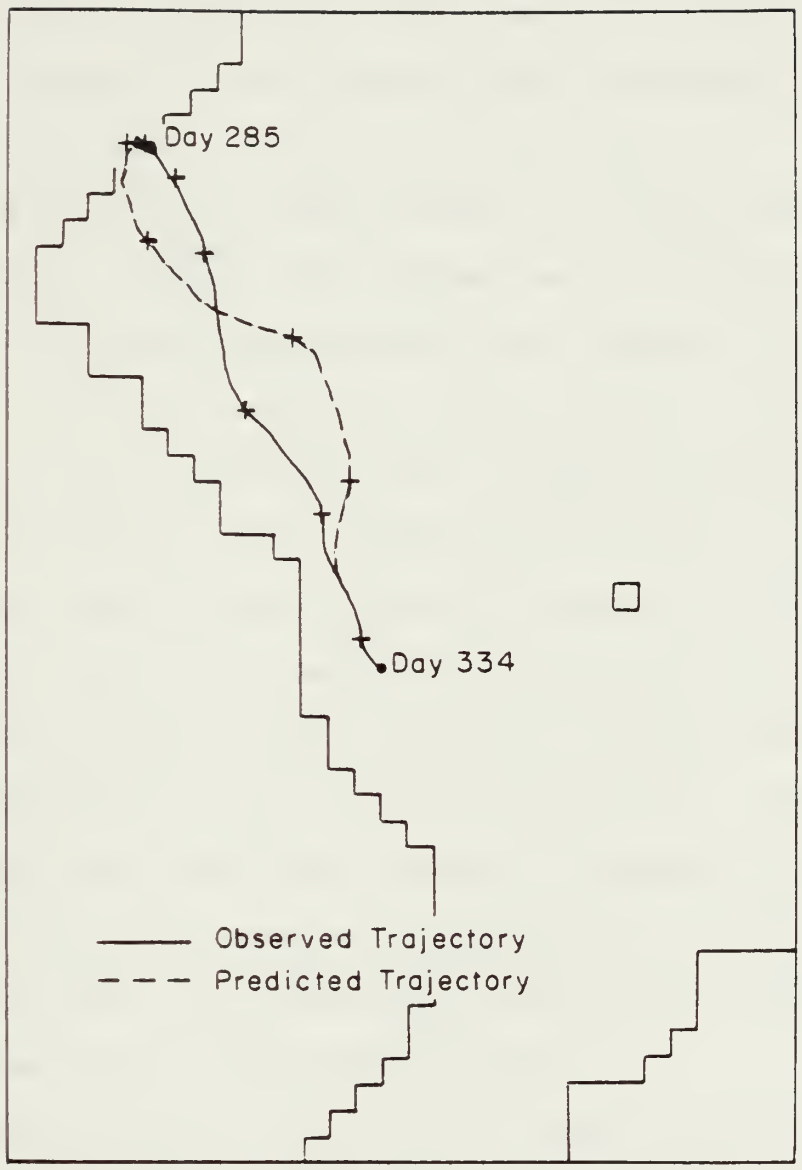

Figure 26. Cumulative daily predicted trajectory for buoy 1564 for the zero currents simulation.

somewhat limited, however, because the effects of current transport can only be examined for the 60-day simulation period. In another modeling study of the arctic ice cover far from shore (Hibler and Tucker, 1979), currents had a negligible short term effect on ice drift but were found to be important in the long term drift. As a result, the feeling was that only a larger magnitude current field would show a significant effect on the ice dynamics for this relatively short term study.

For this simulation, the 60-day averaged ice velocity field generated by the zero current simulation (Fig. 25) was used as a temporally constant current field. The basic idea behind this was to simulate a barotropic oceanic flow in the East Greenland area, where currents would be a two-month average of the ice velocities. This situation is probably not realistic because there is only a relatively narrow region of shallow water adjacent to the coast, and other topographic features in the area (subsea ridges and sills) would not be amenable to barotropic flow. In addition, it is not clear that ocean currents beneath ice covers are entirely driven by stress transmitted into the ocean from the moving ice. Another reason that the averaged ice velocity field was used to simulate the steady current field was because the velocities are generally an order of magnitude higher than those of the geostrophic currents and the sensitivity of the model to much larger currents was of interest.

The 60-day averaged ice velocity field is shown in Figure 27. The effect of the increased current velocities is immediately apparent. Here, ice velocities are much higher than those of the standard run. In some cases, particularly in the area adjacent to the coast, velocities are two to three times larger than those predicted by the standard run (Fig. 7g).

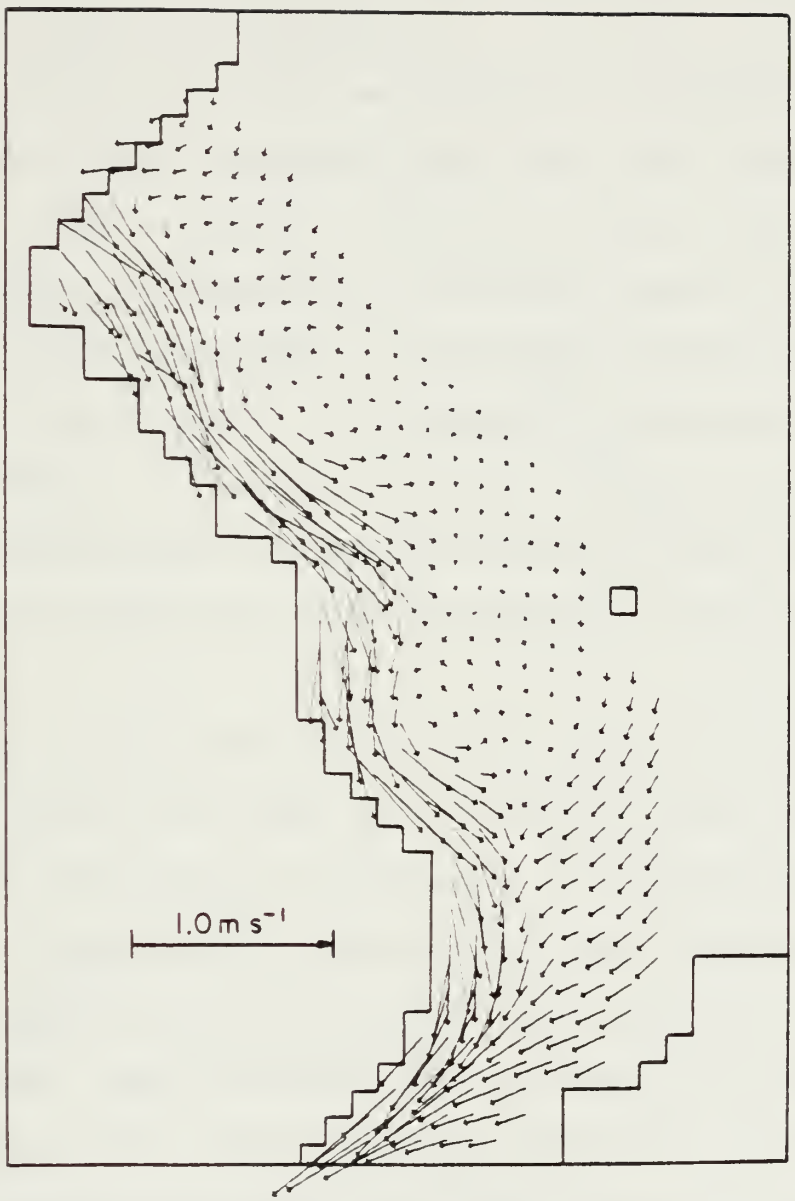

Figure 27. 60-day averaged velocity field for the modified currents simulation.

There appears to be no major direction change, however, except in eastern portions of the northern inflow region where the velocities exhibit a much larger onshore component. Because this was a characteristic of the current field used here, this is not surprising.

The 60-day thickness and compactness contours are presented in Figure 28. Only small differences distinguish these fields from those produced by the standard run (Figs. 5g and 6g). The coastal build-ups, which occur in the same locations as the standard run, are slightly larger. In addition, areas of lower concentration evident in the standard run have even lower compactnesses in this simulation. These can both be attributed to the higher ice velocities. The increased drift can be expected to build ice to higher thicknesses on boundary promontories in the drift path and to lower ice concentrations in their lee, where velocities are moving ice away from the coast.

The cumulative daily predicted trajectory for buoy 1564 is shown in Figure 29. The effect of the higher ice velocities is, again, obvious in this figure, where the predicted final position of the buoy is far southeast of the actual position. The predicted u and v components of velocity correlate with those of the buoy with coefficients of 0.42 and 0.50, respectively. These are somewhat less than those of the standard simulation (0.48 and 0.57), undoubtedly due to the higher velocities. The velocity means significantly reflect these higher velocities, being 0.13 and -0.25 m s^{-1} for the u and v components (0.08 and -0.17 m s^{-1} for the standard run). This is the only simulation in which the magnitudes of the velocity means are larger than the observed component means (0.08 and -0.19 m s^{-1}). Likewise, the RMS errors between the predicted and observed

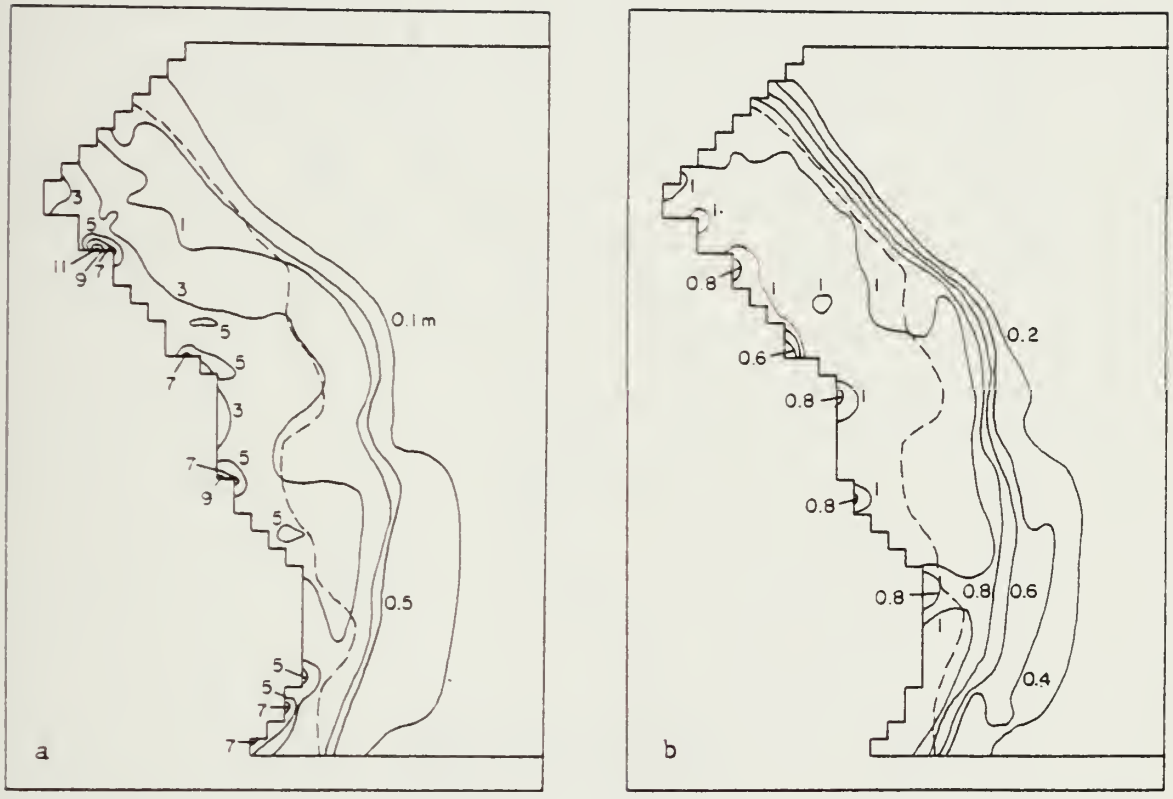

Figure 28. a) 60-day thickness field for the modified currents simulation.
b) 60-day compactness field for the modified currents simulation.
Dashed line is observed ice edge position for 2 December 1979 (NPOC, 1979).

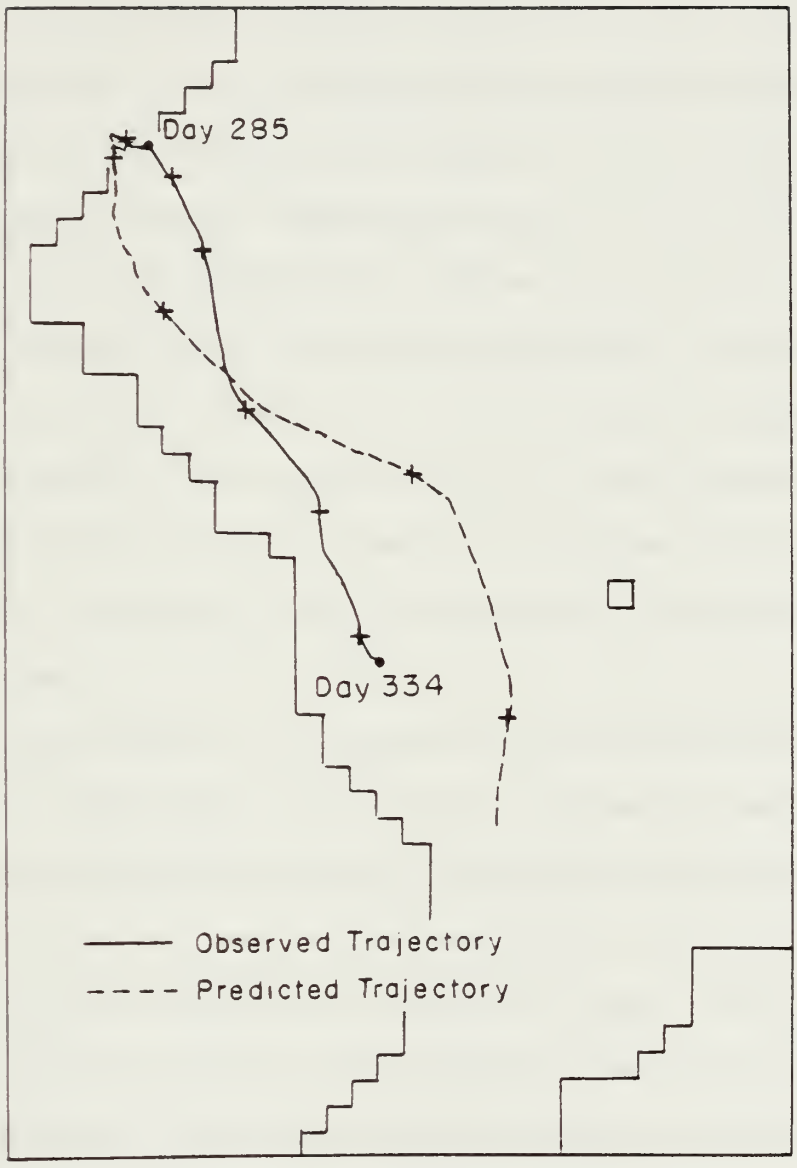

Figure 29. Cumulative daily predicted trajectory for buoy 1564 for the modified currents simulation.

velocity components are larger than in any previous simulation (0.20 and 0.21 m s^{-1}).

The total area of ice cover at the end of the simulation period, 5.88 • 10^{11} m^2, is very similar to that of the standard simulation (5.84 • 10^{11} m^3). This is not surprising because, as previously noted, thermodynamics seem to dominate the areal ice coverage unless significant divergence due to ice dynamics is taking place. The inflow and outflow volumes do show large differences, however. The northern inflow of 7.41 • 10^{11} m^3 is 50% higher than that of the standard run. The southern outflow, 2.94 • 10^{11} m^3, is more than three times that of the standard run. In addition, the total growth for the period was 5.61 • 10^{11} m^3, some 40% higher than the growth that occurred in the standard simulation. This increase in growth may also be attributed to the increased ice velocities, which, in stimulating the overall ice dynamics, created more areas of divergence in which new growth took place.

These results show that the model is indeed very sensitive to the current field in this region. The predicted increase in overall ice transport is rather expected from the order of magnitude increases in current velocities. The results tend to indicate, however, that the current velocities used in this simulation are probably too large. This is implied primarily by the predicted buoy drift trajectory, which places the buoy too far to the southeast, and by the excessive inflow and outflow volumes. Of course, this line of thought assumes that all other model parameters, including the air and water stress drag laws, are reasonable. An appropriate current field for this region will presumably not be available until coupled ice-ocean model studies are undertaken. What would appear to be a

more appropriate current field at this point would seem to be something between the geostrophic field used in previous simulations and the averaged ice velocity field used here.

H. ZERO WINDS

The idea of this simulation was to assess the relative importance of the winds as a driving force in this short term study. It has been previously concluded that the geostrophic currents used in other simulations have only a small impact on the thickness and velocity fields. In addition, a test run in which winds were set to zero and the geostrophic currents alone forced the ice dynamics showed results quite similar to the thermodynamics simulation. Ice velocities were very small, resulting in a northern inflow volume that was only 10% that of the standard simulation. Southern outflow was nonexistent. Because it is suspected that the geostrophic currents may not be representative of actual currents, the modified current field of the previous simulation in which the current field is the 60-day averaged ice velocity field generated by the zero current simulation has been used here. The current velocities, as previously noted, are suspected to be somewhat excessive. In this light, this simulation provides a sort of extreme test of the influence of temporally constant currents on the model results.

Figure 30 presents the 60-day thickness and compactness fields for this zero wind, modified currents simulation. Here, minor effects of the currents on ice dynamics are apparent. In particular, the 3.0-m contour at the inflow boundary and the slightly lower concentrations along the coast are current effects. Also, the ice cover here is slightly more expansive than that generated by the standard or thermodynamics simulations. The

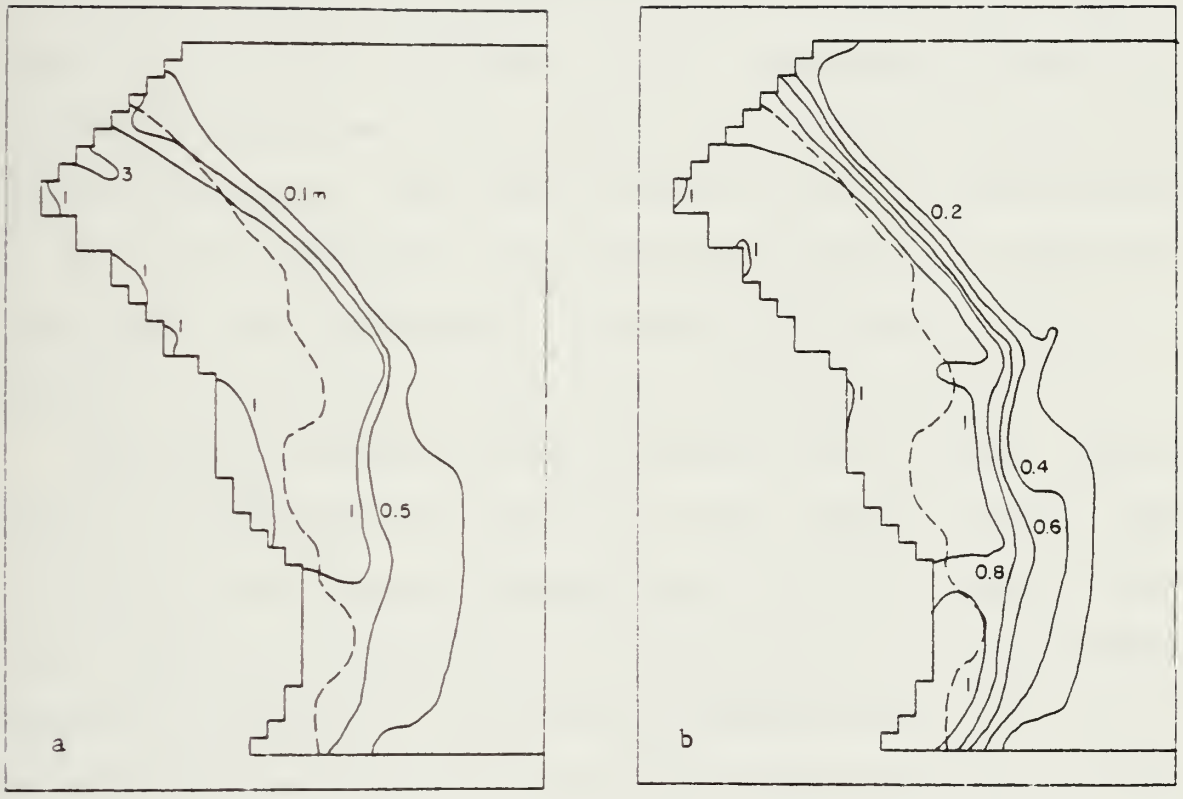

Figure 30. a) 60-day thickness field for the zero winds simulation.
b) 60-day compactness field for the zero winds simulation.
Dashed line is observed ice edge position for 2 December 1979
(NPOC, 1979).

total areal coverage is $6.15 \cdot 10^{11}$ m^2, a 5% increase over the standard run and 10% greater than the thermodynamics simulation. That the ice velocities stimulate this slight expansion is apparent from the 60-day averaged velocity field shown in Figure 31. The expansion is largely in the northern sector of the grid, and it is here that velocities have more of an easterly component than previous simulations have shown.

The velocity field, in particular the stream adjacent to the coast, shows magnitudes that are nearly one-half those of the standard simulation. This is also reflected in the volumes of inflow and outflow ice, whose values are $2.02 \cdot 10^{11}$ m^3 and $0.45 \cdot 10^{11}$ m^3, respectively. These are approximately half those of the standard run, which used the lower velocity geostrophic currents. These values are also about 50% of those produced by the zero current simulation. This indicates that during this period, the model predicts that ice transport by currents (which are felt to be excessive) is on the order of half of that transported by wind.

Expectedly, the cumulative daily predicted drift trajectory, shown in Figure 32, leaves buoy 1564 far shy of its final observed position. This is verified by the v velocity component mean, -0.07 m s^{-1}, which has the lowest magnitude of any simulation and indicates far too little southward transport when compared to the observed v component mean (-0.19 m s^{-1}). The predicted u component mean (0.06 m s^{-1}), on the other hand, is quite comparable to the observed mean (0.08 m s^{-1}). Surprisingly, the u component RMS error is 0.09 m s^{-1}, the lowest of any previous simulation, while the v component RMS error, 0.17 m s^{-1}, is somewhat large. Comparison of the predicted and observed u component velocities (not shown here) revealed that the predicted velocity was nearly constant due to the lack of

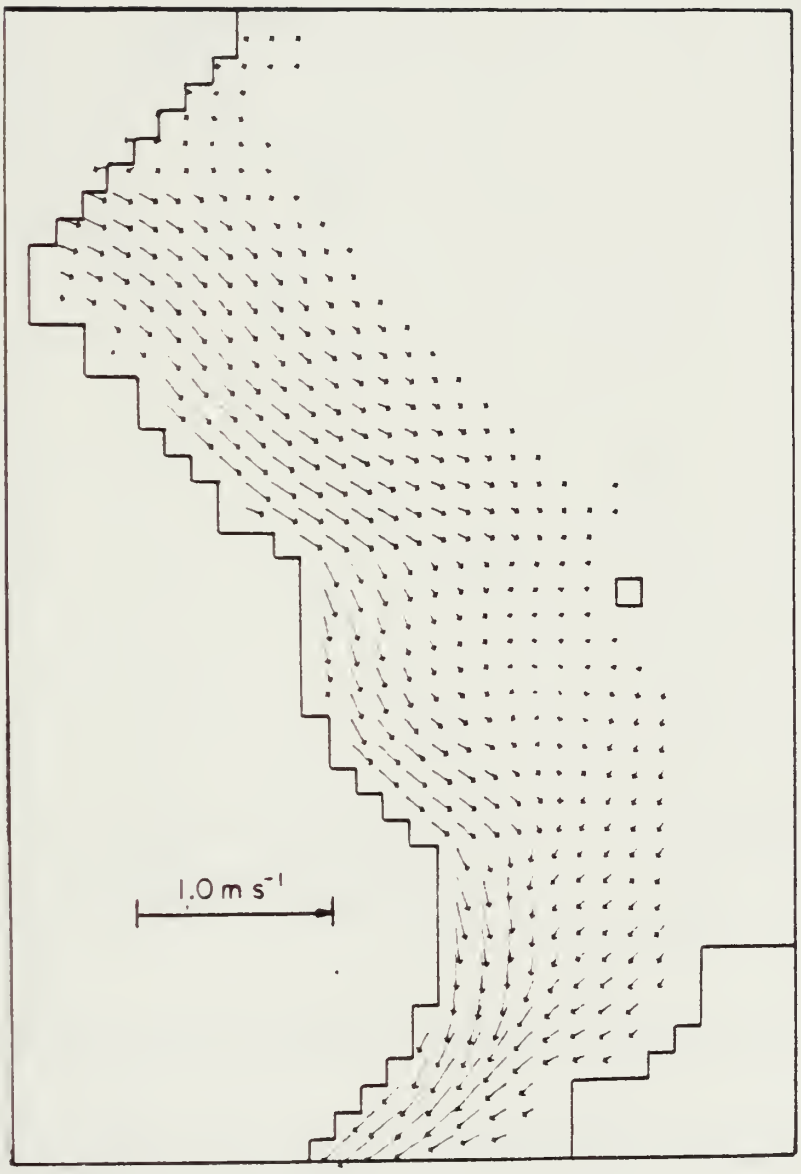

Figure 31. 60-day averaged velocity field for the zero winds simulation.

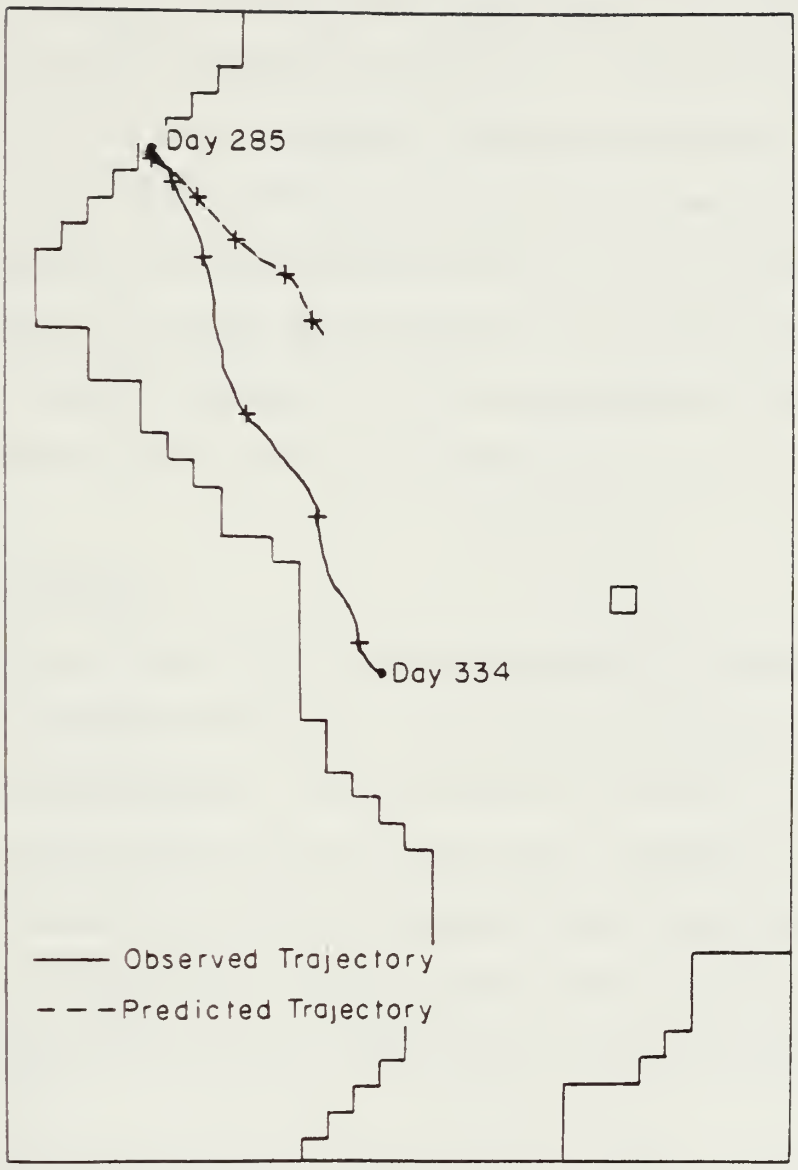

Figure 32. Cumulative daily predicted trajectory for buoy 1564 for the zero winds simulation.

fluctuations caused by the winds. Because the observed magnitudes of the buoy velocity u component are relatively small (Fig. 12), the cumulative squared differences used in the error calculation were less than for other simulations, resulting in a smaller RMS error value. In contrast, the correlation coefficients between the predicted u and v velocity components and those of the buoy are 0.03 and 0.29. These coefficients, which are the lowest of any of the simulations which included ice dynamics, emphasize the day-to-day variation in buoy velocities that can only be accounted for by the wind. This is not to say that currents in this region do not also undergo rapid temporal variations. It is probably safe to assume, however, that the response of the currents to the wind will be less than that of the ice.

I. DYNAMICS SIMULATION

When it became apparent that the thermodynamics was dominating the ice extent in the previous simulations, it was decided to simulate the 60-day period without thermodynamics. The idea here was to see if the ice dynamics alone could enlarge the ice extent, and if significant features caused by ice dynamics in previous simulations were being masked by the overwhelming ice growth. For this simulation, zero growth rates were assigned. Also, the geostrophic current field of earlier simulations was used.

The 60-day thickness and compactness fields which are shown in Figure 33 are rather surprising. The predicted ice edge (0.2 compactness contour) matches the observed ice edge better than in any previous simulation. In addition, the sharp break of the actual ice edge towards the coast near the midpoint of the grid is very well predicted. This feature was somewhat

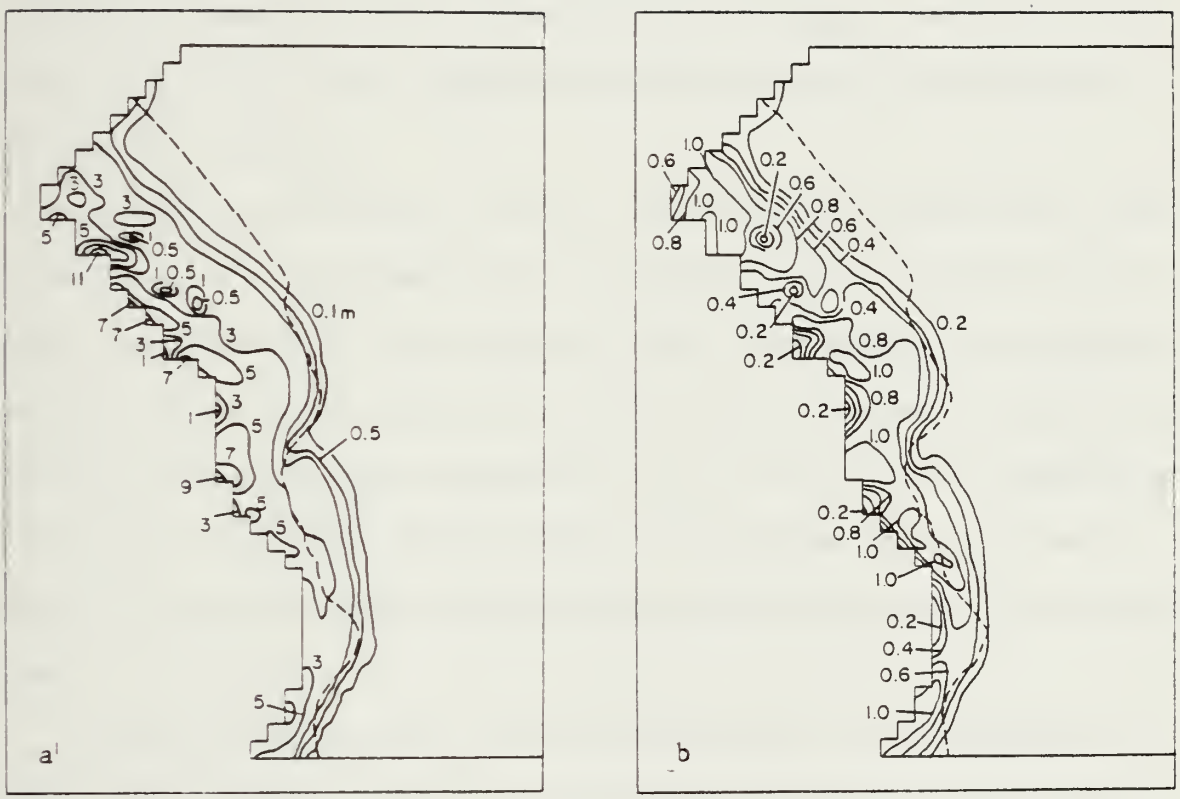

Figure 33. a) 60-day thickness field for the dynamics simulation.
b) 60-day compactness field for the dynamics simulation.
Dashed line is observed ice edge position for 2 December 1979
(NPOC, 1979).

apparent in the 60-day thickness field produced by the standard run (Fig. 5g), but was partially obscured by the new ice growth. Here it is clear that this feature in the observed ice edge is probably a result of ice dynamics.

That too little ice is present in the north is almost certainly a result of no ice growth. The excess of ice in the south is an unresolved problem, but two possibilities exist. First, the simulated ice dynamics may not be adequately reproducing the actual ice dynamics in this area, due to improper winds, currents, or possibly ice rheology. The other possibility is that the ocean significantly ablated the ice in this region during this time period.

The thickness build-ups along the coast are more numerous than those of the standard run, presumably due to slightly higher velocities. This figure also shows many smaller areas of lower concentration and thickness, however, because new ice growth was not allowed to proceed. Offshore velocities and subsequent mass divergence in the lee of boundary promontories appear to be responsible for the lower concentrations along the coast. Away from the coast, excessive advection out of cells creates the divergent areas.

In light of the superior ice extent prediction, it is meaningful to again provide a table of total ice coverage as has been done previously. Table III shows the total areal coverage for the dynamics simulation at 10 day intervals, the percentage change during intervals, and the percent difference between this simulation's predictions, the observations and the standard run.

Table III. Predicted areas (in 10^{11} m^2) of ice cover for the dynamics simulation for 10 day intervals with the percent difference between this simulation and the observed coverage and the standard simulation.

	Predicted	% Difference from Observed	% Difference from Standard Run
Initial Area	1.80		
Area Day 10	1.65	-25.3	-12.2
Change (%)	-8.3		
Area Day 20	1.83	-18.3	-48.4
Change (%)	10.9		
Area Day 30	1.85	-10.2	-45.2
Change (%)	1.1		
Area Day 40	1.98	-15.0	-47.8
Change (%)	7.0		
Area Day 50	2.26	- 8.9	-49.7
Change (%)	14.1		
Area Day 60	2.37	-24.2	-59.4
Change (%)	4.9		

Generally, differences between the dynamics simulation predicted coverage and the observed coverage are far less than those of the standard simulation. As expected from previous figures, the extent of ice is also far less than that simulated by the standard run. The less-than-observed extents predicted here do indicate, however, that ice growth is necessary for a reasonable simulation. This is made quite obvious by the particularly large differences between the simulated and observed extents on day 60. Likewise, the large expansion of the ice cover that actually took place between days 50 and 60 (26% increase) appears to be primarily due to ice growth. The thermodynamic simulation predicted such an increase (30%), but the ice cover in that simulation was already excessive on day 50 and the increase extended the cover too far eastward.

The implication here has been made previously. This simulation verifies that both dynamics and thermodynamics are important to obtain reason-

able ice extents in this region. The thermodynamics used for these simulations need considerable improvement, however. It seems that the major improvement to be made will be an adequate specification of oceanic heat flux. That the thermodynamic code is adequate for the Arctic Basin has been shown by Hibler (1980b). In that study, oceanic boundary layer heat storage was allowed and the simulation provided very reasonable results. In the East Greenland area, perhaps both boundary layer heat storage and the advection of warmer waters from the south need to be parameterized for an adequate thermodynamic model.

The 60-day averaged velocities, shown in Figure 34, look similar to those of the standard run (Fig. 7g) except for areas near the eastern side of the high velocity stream. In the region of the sharp break toward the coast, an onshore velocity component exists. In previous simulations, higher thicknesses in this region presumably prevented this onshore component. Velocities within the stream itself also appear to be slightly higher, but these differences are difficult to discern from these figures.

The predicted u and v velocity component means for buoy 1564, 0.08 and -0.18 m s^{-1}, exceed those in any previous simulation as far as comparison to the observed component means (0.08 and -0.19 m s^{-1}) is concerned. In addition, the RMS errors for the velocity components are quite reasonable, being 0.13 and 0.14 m s^{-1}. The u component error is 0.01 m s^{-1} higher than that for the standard run while the v component error is the same as in the standard simulation. In the correlation of predicted velocities with those of buoy 1564, the u and v coefficients are 0.49 and 0.53. These coefficients represent a slightly higher value for the u component and a lower value for the v component than in the standard run (0.48, 0.57) but, in

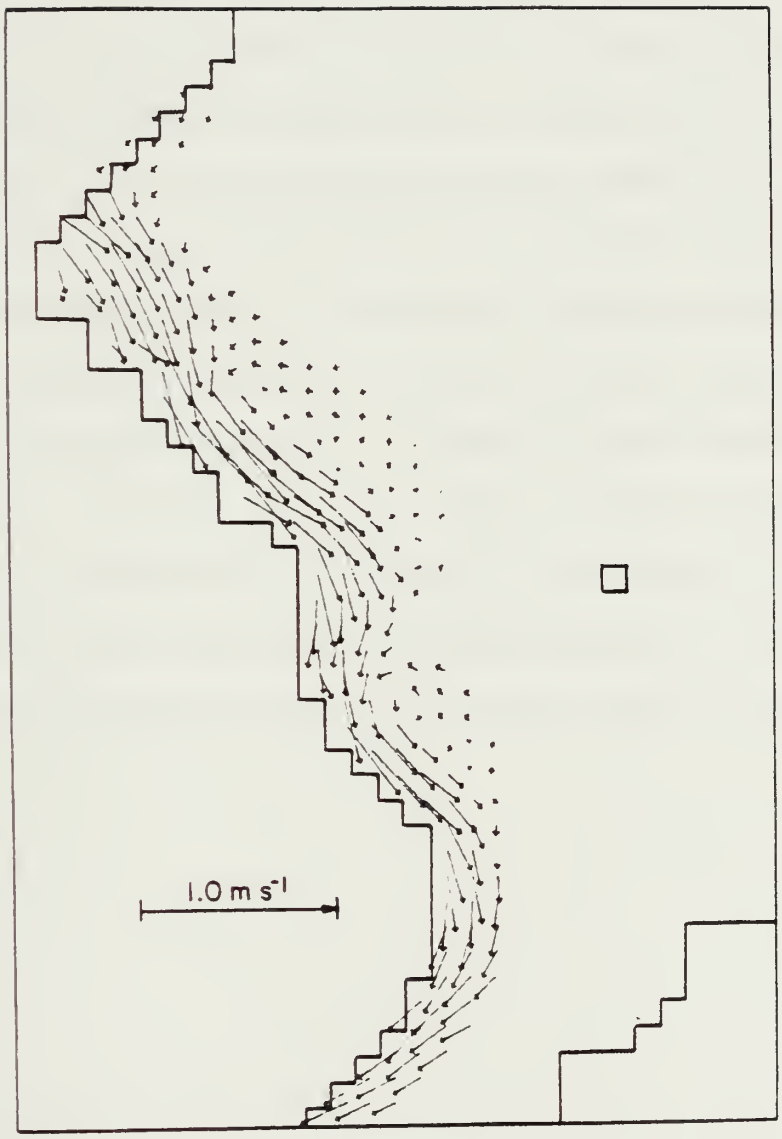

Figure 34. 60-day averaged velocity field for the dynamics simulation.

general, are in the same range as the other simulations. The velocity differences become more apparent in the cumulative daily predicted trajectory of this buoy, shown in Figure 35. This trajectory is better than that obtained in any other simulation with respect to final position. This is probably accounted for by slightly higher velocities overall.

The dynamics simulation predicts a 14% larger volume of northern inflow ice than the standard run, $5.39 \cdot 10^{11}$ m^3. This is no surprise in that larger velocities would be expected in the inflow region because of lower strength ice. The lower strengths presumably result from lower thicknesses due to the lack of ice growth. The southern outflow, on the other hand, differs considerably. The dynamics simulation produces $0.32 \cdot 10^{11}$ m^3 while the standard run predicts two-and-one-half times this amount. This is obviously a result of the lack of thermodynamics, whose effect is twofold. Initially, ice growth acts to "fill" the region with ice quite rapidly (too rapidly) and outflow for the standard run can begin at an earlier time. In addition, the continuing growth of ice makes considerably more ice available for outflow during the entire simulation period.

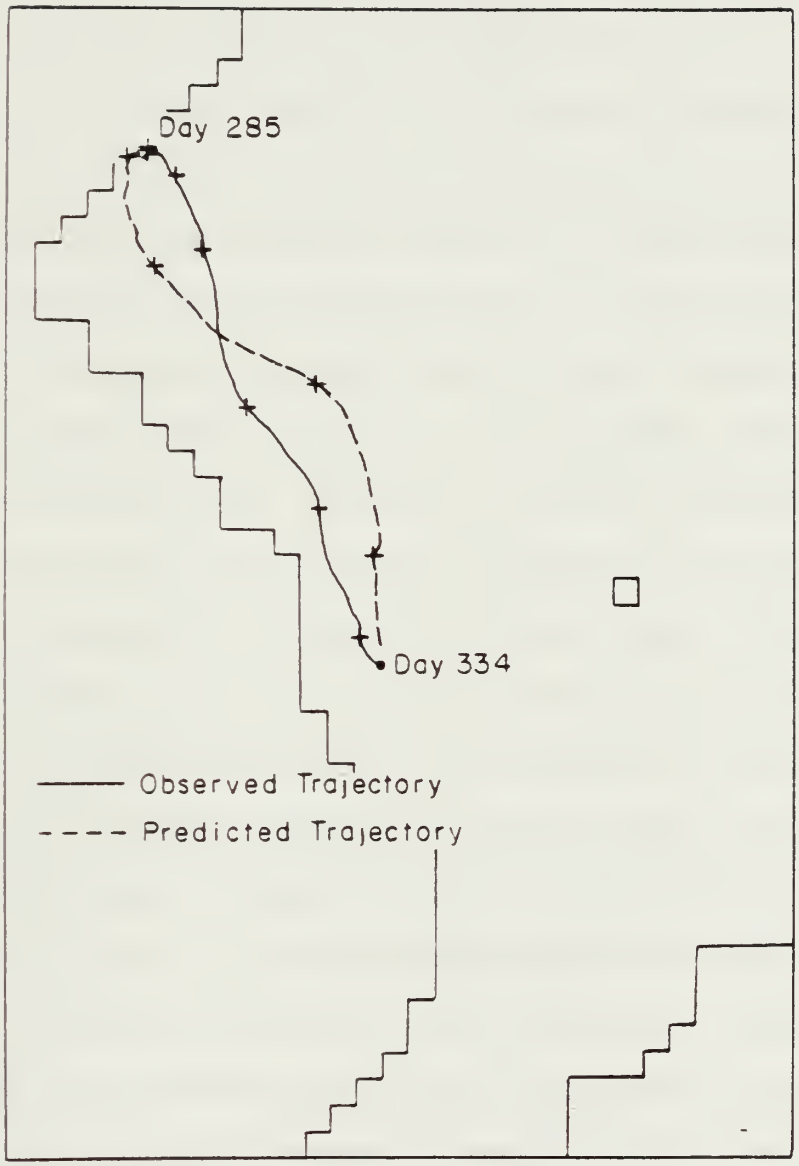

Figure 35. Cumulative daily predicted trajectory for buoy 1564 for the dynamics simulation.

IV. SUMMARY AND CONCLUDING REMARKS

Pertinent mass balance results from the various simulations are presented in Table IV. Velocity comparison statistics for each simulation are summarized in Table V. Most of these have been previously discussed but are repeated here for the sake of ease of comparison.

By far the most radical statistics are yielded by the zero strength simulation. Total ice growth, as previously mentioned, is two orders of magnitude higher than that predicted by any of the other simulations. This is presumably produced by the continuing cycle of rapid advection and subsequent thin ice growth in specific areas. From a different perspective, the free drift condition causes the ice to respond nearly instantaneously to rapidly varying winds, regardless of the ice thickness. In other simulations, this effect is diminished by allowing the ice to have strength. This results in a more uniform velocity field. While areas of divergence can still occur, it is only after periods of sustained wind forcing that ice is moved into areas of less strength. Another surprising result of the zero strength simulation is that net inflow took place in the southern boundary region, although this is not apparent from the averaged velocity field (Fig. 20). A detailed examination of the results resolved this problem. During the latter part of the simulation, reasonably thick ice had accumulated adjacent to the coast in this boundary region. In addition, a slight northward component of velocity was evident for several grid points in that area. As a result, this small northward drift moved the very thick ice back into the grid and a net inflow in this region was

Table IV. Model sensitivity test mass balance results.

	Northern Inflow ($10^{11} m^3$)	Southern Outflow ($10^{11} m^3$)	Total Growth ($10^{11} m^3$)	Total Ice Increase ($10^{11} m^3$)	60-Day Areal Coverage ($10^{11} m^2$)
Standard	4.73	0.83	3.95	7.85	5.84
Thermodynamics	0.0	0.0	2.57	2.57	5.5o
Zero strength	6.18	-1.11	155.56	162.85	4.47
Zero inflow	0.0	0.83	5.62	4.77	5.56
Zero currents	3.85	0.81	4.11	7.16	5.78
Modified currents	7.41	2.94	5.61	10.08	5.88
Zero winds	2.02	0.45	2.74	4.31	6.15
Dynamics	5.39	0.32	0.0	5.07	2.37

Table V. Simulated velocity comparisons with buoy 1564.

	Predicted Mean* ($m\ s^{-1}$)		RMS Error ($m\ s^{-1}$)		Correlation Coefficient	
	u	v	u	v	u	v
Standard	0.08	-0.17	0.12	0.14	0.48	0.57
Zero strength	-0.03	-0.17	0.16	0.16	0.45	0.45
Zero inflow	0.06	-0.16	0.14	0.15	0.48	0.52
Zero currents	0.07	-0.15	0.12	0.14	0.47	0.54
Modified currents	0.13	-0.25	0.20	0.21	0.42	0.50
Zero winds	0.06	-0.07	0.09	0.17	0.03	0.29
Dynamics	0.08	-0.18	0.13	0.14	0.49	0.53

* The observed u and v means are 0.08 and -0.19 $m\ s^{-1}$.

created. The essence of this simulation is that the zero strength condition allows the forcing fields to move unreasonably large amounts of ice. It is apparent that an ice strength that is at least partially dependent on thickness is necessary to obtain reasonable ice thicknesses and compactnesses.

The thermodynamics simulation made it clear that ice growth alone was responsible for creating too large an area of ice cover. It became apparent in this simulation that the oceanic heat flux needs to be

considered to properly model ice growth in this region. Comparison of the total growth in this simulation with that produced in the standard run also shows that ice growth is further stimulated by ice dynamics. This fact may have a significant effect on air-sea energy exchange in this region. For this reason, and for the obvious reason that ice transport and drift cannot be predicted with a pure thermodynamic ice model, the inclusion of ice dynamics in any modeling effort for this region is deemed necessary.

The zero inflow simulation emphasizes the importance of ice transport from the Arctic Basin into the East Greenland Sea. Although the areal coverage is not significantly different from that predicted by the standard simulation, the thickness and compactness fields (Fig. 22) and the total ice volume increase are quite different. No impact upon the volume of southern outflow is noted, but a longer simulation would likely show discernible differences. Reasonable ice velocities are maintained in this simulation, and as a result, total growth is larger than that of the standard run. This is due primarily to the rapid advection and subsequent growth in the northern sector where velocities are larger. The salient point of this simulation is that a reasonable thickness regime cannot be maintained without ice inflow which, when corrected for outflow, supplied approximately half the total ice volume increase during this period (according to the standard run).

The zero currents simulation sheds light on the fact that the geostrophic currents used in other simulations contribute little to the ice dynamics except to the volume of inflow ice. In view of previous investigations reviewed earlier, it is suspected that the geostrophic current velocities are too small. On the other hand, using the average ice veloc-

ity field as a current field creates excessive ice velocities. These large velocities greatly increase inflow, outflow and ice growth to levels that are probably also unreasonable. What these two simulations tend to point out is that if all other model parameters are reasonable, then the currents in this region are neither purely geostrophic (also assuming the geostrophic currents here are reasonable) nor totally ice-driven. This is not unexpected, and future work at some point should address a coupled ice-ocean model.

The zero winds simulation, which uses the modified current field to create an extreme case, clearly shows that winds are the major driving force during this simulated time period. Even with the excessive currents, the total transport (inflow and outflow) is about half that simulated by winds alone. Daily winds are also necessary to predict reasonably accurate velocities, as noted from the large daily variations in actual buoy velocities. Although it appears that ice dynamics can be reasonably simulated without currents for short time periods, these results imply that they cannot be properly simulated without winds.

That ice growth has been excessive in previous simulations is verified by the dynamics-only case. In this simulation the best agreement between the observed and predicted ice extent is obtained. From the 60-day thickness and compactness contour plot (Fig. 31) it is obvious, however, that growth is necessary in the north, and more ablation is needed in the southern region to obtain a better predicted areal extent. The volume of inflow ice in this simulation appears excessive. As was apparent from the standard simulation, growth in the northern sector sufficiently increased thickness, which decreased velocities and suppressed inflow. The southern

outflow volume here is approximately 40% of that in the standard run. It is suspected that this value is the more reasonable, due primarily to excessive ice extent in the south when growth is allowed to proceed.

The problems with the model results, in particular referring to the standard run, have yet to be resolved. As noted on several occasions, these major problems are excessive ice growth and improper ice velocities in the vicinity of the ice edge. Future work will focus on the resolution of these problems within guidelines previously mentioned. In addition, simulations will be carried out for different seasons and hopefully for longer periods (90-120 days).

In spite of these problems, however, this study has shed light on several key issues concerning modeling studies in the East Greenland area. Without hesitation, the most important is that a sea ice model which utilizes a viscous-plastic constitutive law as developed by Hibler (1979) seems to provide reasonable results over most of the region. Furthermore, this investigation points out the necessity of using a coupled dynamic-thermodynamic model to properly model this region. The importance of including ice dynamics in studies of air-sea energy exchange has previously been emphasized. Allowing the ice to have strength and to interact with itself is a necessity that has also been clarified by this study. In addition, it has been shown that winds, currents and ice import from the Arctic Basin all contributed significantly to the ice balance, even during this short study period.

Detailed model refinement will be difficult without a significant increase in the amount and quality of the observational data. In particular, future studies will require more ice drift data and more detailed

thickness and concentration information. The relatively sparse data set used in this study has been sufficient to point out certain model deficiencies and to draw general conclusions. The model can also be further refined to a limited degree (i.e. thermodynamics and possibly ice velocities) with the currently available data. However, the refinements necessary to "tune" the model for operational forecasting use will certainly require more detailed data during all seasons.

REFERENCES

Aagaard, K., 1972: On the drift of the Greenland pack ice. In Sea Ice (T. Karlsson, ed.), Nat. Res. Counc. of Iceland, Reykjavik, 17-22.

Aagaard, K. and L.K. Coachman, 1968: The East Greenland Current north of the Denmark Strait: Part II. Arctic, 21(4), 267-290.

Aagaard, K. and P. Greisman, 1975: Toward new mass and heat budgets for the Arctic Ocean. J. Geophys. Res., 80, 3821-3827.

Antropova, L.V. and B.A. Kogan, 1977: Calculating basic components of ice balance in the Denmark Strait. In Natural Conditions and Resources of Northern Seas (V.T. Zhernovatyi, ed.), 90-107.

Diachok, O.I. and R.S. Winokur, 1974: Spatial variability of underwater ambient noise at the Arctic ice-water boundary. J. Acous. Soc. Am., 55, 750-753.

Einarsson, Tr., 1972: Sea currents, ice drift and ice composition in the East Greenland Current. In Sea Ice (T. Karlsson, ed.), Nat. Res. Counc. of Iceland, Reykjavik, 23-32.

Hibler, W.D. III, 1979: A dynamic thermodynamic sea ice model. J. Phys. Oceanogr., 9, 815-846.

Hibler, W.D. III, 1980a: Documentation for a two-level dynamic thermodynamic sea ice model. Special Report 80-8, U.S. Army Cold Regions Research and Engineering Laboratory, Hanover, N.H., 1-35.

Hibler, W.D. III, 1980b: Modeling a variable thickness sea ice cover. Mo. Wea. Rev., (108)12, 1944-1973.

Hibler, W.D. III and W.B. Tucker III, 1979: Some results from a linear-viscous model of the arctic ice cover. J. Glaciol., 22(87), 293-304.

Karlsson, T., 1969: Sea ice drift in the East Greenland Current. Jökull, 19 Ar, 53-61.

Kelly, P.M., 1978: Forecasting the arctic sea ice on time scales of a few months to many years. Clim. Monit., 7(3), 95-98.

Kiilerich, A., 1945: On the hydrography of the Greenland Sea. Medd. om Gron., 144(2).

Kloster, K. and J. Rafto, 1980: ICEX-Project, Data from drifting buoys north and west of Svalbard in the fall of 1979. Report of Chr. Michelsen Institute, 1-13.

Kozo, T.L. and O.I. Diachok, 1973: Spatial variability of topside and bottomside ice roughness and its relevance to underside acoustic reflection loss. AIDJEX Bulletin, 19, 113-121.

Kozo, T.L. and W.B. Tucker, 1974: Sea ice bottomside features in the Denmark Strait. J. Geophys. Res. 79(30), 4505-4511.

Lebedev, A.A. and N.S. Uralov, 1976: Experiment on estimating sea ice area from ice balance components (using the East Greenland ice zone as an example). Trudy Ark. Antark. Nauch. Issled. Inst., 320, 65-82.

Nansen, F., 1924: Blant sael og björn Kria.

Naval Polar Oceanography Center, 1979: Eastern-western Arctic sea ice analysis - 1979. Naval Polar Oceanography Center, Washington, D.C.

Roed, L.P. and J.J. O'Brien, 1981: Geostrophic adjustment in a highly dispersive media: An application to the marginal ice zone. Submitted to: J. of Geophys. Astrophys. Fluid Dyn.

Sanders, F. and J.R. Gyakum, 1980: Synoptic-dynamic climatology of the "bomb." Mo. Wea. Rev., 108, 1589-1606.

Sanderson, R.M., 1971: Ice edge in the Greenland Sea. Mar. Ob., 41(234), 173-183.

Skov, N.A., 1970: The ice cover of the Greenland Sea. An evaluation of oceanographic and meteorological causes for year-to-year variations. Medd. om Grön., 2, 1-56.

Stefansson, U., 1962: North Icelandic waters. Rit Fiskideildar, Vol. II, Reykjavik.

Thorndike, A.S. and R. Colony, 1980: Arctic Ocean buoy program data report: 19 January 1979-31 December 1979. Polar Science Center, University of Washington, Seattle, Washington, 1-131.

Tucker, W.B. III and W.D. Hibler III, 1981: Preliminary results of ice modeling in the East Greenland area. Proc. of POAC-81, 27-31 July, 1981, Quebec, Canada.

Vinje, T.E., 1972: Sea ice drift and speed observations in 1970. Norsk Polarinstitutt Arbok 1970, 256-263.

Vinje, T.E., 1973: Sea ice drift and speed observations in 1971. Norsk Polarinstitutt Arbok 1971, 81-85.

Vinje, T.E., 1977: Sea ice conditions in the European sector of the marginal seas of the Arctic 1966-1975. Norsk Polarinstitutt Arbok 1975, 163-174.

Vinje, T.E., 1981: The drift pattern of sea ice in the Arctic with particular reference to the Atlantic approach. In The Arctic Ocean: The Hydrographic Environment and the Fate of Pollutants (Louis Rey, ed.) in press.

Vowinckel, E., 1964: Ice transport in the East Greenland Current and its causes. Arctic 17(2), 111-119.

Wadhams, P., 1980a: Ice characteristics in the seasonal sea ice zone, Cold Reg. Sci. Tech., 2, 39-87.

Wadhams, P., 1980b: A comparison of sonar and laser profiles along corresponding tracks in the Arctic Ocean. In Sea Ice Processes and Models (R.S. Pritchard, ed.), 283-299.

Wadhams, P., 1981: The ice cover in the Greenland and Norwegian Seas. Rev. Geophys. Space Phys., 19(3), 345-393.

Wadhams, P., A.E. Gill and P.F. Linden, 1979: Transects by submarine of the East Greenland Polar Front. Deep-Sea Res., 26(12A), 1311-1328.

Walsh, J.E. and C.M. Johnson, 1979: Interannual atmospheric variability and associated fluctuations in arctic sea ice extent. J. Geophys. Res., 84(C11), 6915-6928.

Zubov, N.N., 1945: Arctic Ice. Moscow: Izd. Glavs., 1-360.

INITIAL DISTRIBUTION LIST

		No. Copies
1.	Defense Technical Information Center Cameron Station Alexandria, Virginia 22314	2
2.	Library, Code 0142 Naval Postgraduate School Monterey, California 93940	2
3.	Chairman (Code 68Mr) Department of Oceanography Naval Postgraduate School Monterey, California 93940	1
4.	Chairman (Code 63Rd) Department of Meteorology Naval Postgraduate School Monterey, California 93940	1
5.	Prof. R. G. Paquette (Code 68Pa) Department of Oceanography Naval Postgraduate School Monterey, California 93940	1
6.	Prof. R. L. Haney (Code 63Hy) Department of Meteorology Naval Postgraduate School Monterey, California 93940	1
7.	W. B. Tucker III U.S. Army Cold Regions Research and Engineering Laboratory 72 Lyme Road Hanover, New Hampshire 03755	2
8.	Director Naval Oceanography Division Naval Observatory 34th and Massachusetts Avenue NW Washington, D.G. 20390	1
9.	Commander Naval Oceanography Command NSTL Station Bay St Louis, Mississippi 39522	1

10. Commanding Officer — 1
Naval Oceanography Office
NSTL Station
Bay St Louis, Mississippi 39522

11. Commanding Officer — 1
Fleet Numerical Oceanography Center
Monterey, California 93940

12. Commanding Officer — 1
Naval Ocean Research and Development Activity
NSTL Station
Bay St Louis, Mississippi 39522

13. Commanding Officer — 1
Naval Environment Prediction Research Facility
Monterey, California 93940

14. Chairman, Oceanography Department — 1
U. S. Naval Academy
Annapolis, Maryland 21402

15. Chief of Naval Research — 1
800 North Quincy Street
Arlington, Virginia 22217

16. Office of Naval Research (Code 420) — 1
Naval Ocean Research and Development Activity
NSTL Station
Bay St Louis, Mississippi 39522

17. Arctic Program (Code 428) — 1
ATTN: Dr. Leonard Johnson
Office of Naval Research
800 North Quincy Street
Arlington, Virginia 22217

18. Arctic Program (Code 428) — 1
ATTN: Mr. Ronald McGregor
Office of Naval Research
800 North Quincy Street
Arlington, Virginia 22217

19. Commanding Officer — 1
Naval Polar Oceanography Center
Navy Department
4301 Suitland Road
Washington, D.C. 20390

20. Commanding Officer 1
ATTN: Mr. Donald Barnett
Naval Polar Oceanography Center
Navy Department
4301 Suitland Road
Washington, D.C. 20390

21. Library 1
U.S. Army Cold Regions Research
and Engineering Laboratory
72 Lyme Road
Hanover, New Hampshire 03755

22. Office of Naval Research 1
ATTN: Mr. Ben Cagle
1030 East Green Street
Pasadena, California 91106

Thesis
T8465 Tucker
c.1 An application of a numerical sea ice model to the East Greenland area.